

Target selection by frontal cortex during coordinated saccadic and smooth pursuit eye movements

Krishna Srihasam, Daniel Bullock, & Stephen Grossberg¹

Department of Cognitive and Neural Systems
and
Center for Adaptive Systems
Boston University
677 Beacon Street, Boston, MA 02215
Phone: 617-353-7858
Fax: 617-353-7755

Technical Report CAS/CNS TR-2007-019
Submitted: November 27, 2007

All correspondence should be addressed to
Professor Stephen Grossberg
Department of Cognitive and Neural Systems
Boston University
677 Beacon Street
Boston, MA 02215
Phone: 617-353-7858
Fax: 617-353-7755
Email: steve@bu.edu

¹ Authorship is in rotated alphabetical order. DB, SG and KS were supported in part by NSF grant SBE-0354378. SG was also supported in part by the office of Naval Research (ONR N00014-01-1-0624).

Abstract

Oculomotor tracking of moving objects is an important component of visually based cognition and planning. Such tracking is achieved by a combination of saccades and smooth pursuit eye movements. In particular, the saccadic and smooth pursuit systems interact to often choose the same target, and to maximize its visibility through time. How do multiple brain regions interact, including frontal cortical areas, to decide the choice of a target among several competing moving stimuli? How is target selection information that is created by a bias (e.g., electrical stimulation) transferred from one movement system to another? These saccade-pursuit interactions are clarified by a new computational neural model, which describes interactions between motion processing areas MT, MST, FPA, DLPN; saccade specification, selection, and planning areas LIP, FEF, SNr, SC; the saccadic generator in the brain stem; and the cerebellum. Model simulations explain a broad range of neuroanatomical and neurophysiological data. These results are in contrast with the simplest parallel model with no interactions between saccades and pursuit than common-target selection and recruitment of shared motoneurons. Actual tracking episodes in primates reveal multiple systematic deviations from predictions of the simplest parallel model, which are explained by the current model.

Introduction

The primate retina affords wide-field detection of visual pattern and motion, as well as narrow-field scrutiny of visual details via its central zone, the fovea. A typical oculomotor episode involves detection of visual stimuli by receptors in the retinal periphery, cortical selection of one of the detected stimuli as a goal for scrutiny, and genesis of eye movements that enable foveation of the goal. Two eye movement systems cooperate to achieve foveation if the goal stimulus is moving: SAC and SPEM. The saccadic (SAC) eye movement system generates ballistic, high-velocity, open loop, ocular rotations that quickly cancel the difference between the initial angle of gaze and the angle needed to foveate the goal. The smooth pursuit eye movement (SPEM) system generates continuous, moderate velocity, closed-loop, ocular rotations that prolong foveation of mobile goal stimuli by trying to match gaze velocity to stimulus velocity. For sufficiently fast stimuli, prolonged foveation requires re-engagement of the SAC system to generate “catch-up” saccades.

It is critical that the two eye movements systems coordinate, so that they (1) choose the same target as the goal for future movement, and (2) maximize visibility of that target. A prior report (Grossberg, Srihasam, & Bullock, 2007) introduced a new model of SAC-SPEM interactions, and reported data-simulation comparisons that revealed how the model achieved the second of these requirements. This report presents additional simulation-data comparisons which illustrate how circuit interactions ensure that both systems generate movements directed to the same target.

It might be thought that unitary targeting is not a significant problem. However, one system can operate without the other, a typical scene contains an assortment of salient stimuli with some stationary and some moving, and the motion-sensitive anatomical pathways that generate SPEM are largely separate from, and evolved after, those that generate SAC (Krauzlis, 2005; Krauzlis, Liston, & Carello, 2004). What interactions choose a unitary goal among several competing stimuli? Is goal selection information transferred from one system to the other, and if so, how?

Although SAC and SPEM systems have often been assumed to have a single, shared, target selection mechanism, recent data from monkeys suggest that each system has a selection mechanism that can operate independently of the other. In these experiments, two different stimuli appear and begin to move in different directions. Location, shape, direction of motion, or color help the monkey distinguish a task-relevant target from an irrelevant distractor (Adler et al., 2002; Ferrera & Lisberger, 1995; Garbutt & Lisberger, 2006; Gardner & Lisberger, 2001; Krauzlis et al., 1999). Because the latency for SPEM initiation is shorter than for SAC initiation, it is possible to behaviorally assess whether the SPEM system always reflects the same choice as the slower-starting SAC system. Indeed, on a substantial fraction of trials, the *initial* SPEM tracks the distractor. However, immediately after a saccade to the correct target, the *continuing* SPEM tracks that target rather than the distractor. Such results suggest that each of the SAC and SPEM systems makes its own initial choice of goal, but that the SAC choice overrides the SPEM system’s choice (Adler et al., 2002; Ferrera & Lisberger, 1995; Gardner & Lisberger, 2001, 2002; Horwitz & Newsome, 2001).

Before the model of Grossberg et al. (2007), no model had addressed the functional anatomy of SAC-SPEM interactions for target selection and coordination. While a lot is known about the mechanisms involved in saccadic target selection (Arai et al., 2002; Basso & Wurtz, 2002; Krauzlis, Liston & Carello, 2004; McPeck & Keller, 2002; Schall, Hanes et al., 1995; Schiller & Tehovnik, 2003, 2005; Thompson et al., 1996; Thomas & Pare, 2007), less is known about how

smooth pursuit target selection occurs (Case & Ferrera, 2007; Garbutt & Lisberger, 2006; Krauzlis, 2005), or about how these two eye movement systems interact to select the same target among many distractors (Adler et al., 2002; Gardner & Lisberger, 2001, 2002; Krauzlis et al., 1999). Our new model proposes a mechanistic explanation for, and quantitatively simulates, the key generalizations that have emerged from systematic empirical studies of target tracking eye movements concerning how the smooth pursuit system selects its target, and how the two eye movement systems interact to select the same target. After reviewing the SAC-SPEM model's circuitry and operation, the present paper explains how model circuits, notably those dependent on the frontal cortex, can explain and simulate challenging behavioral and electrophysiological data from experiments on target selection.

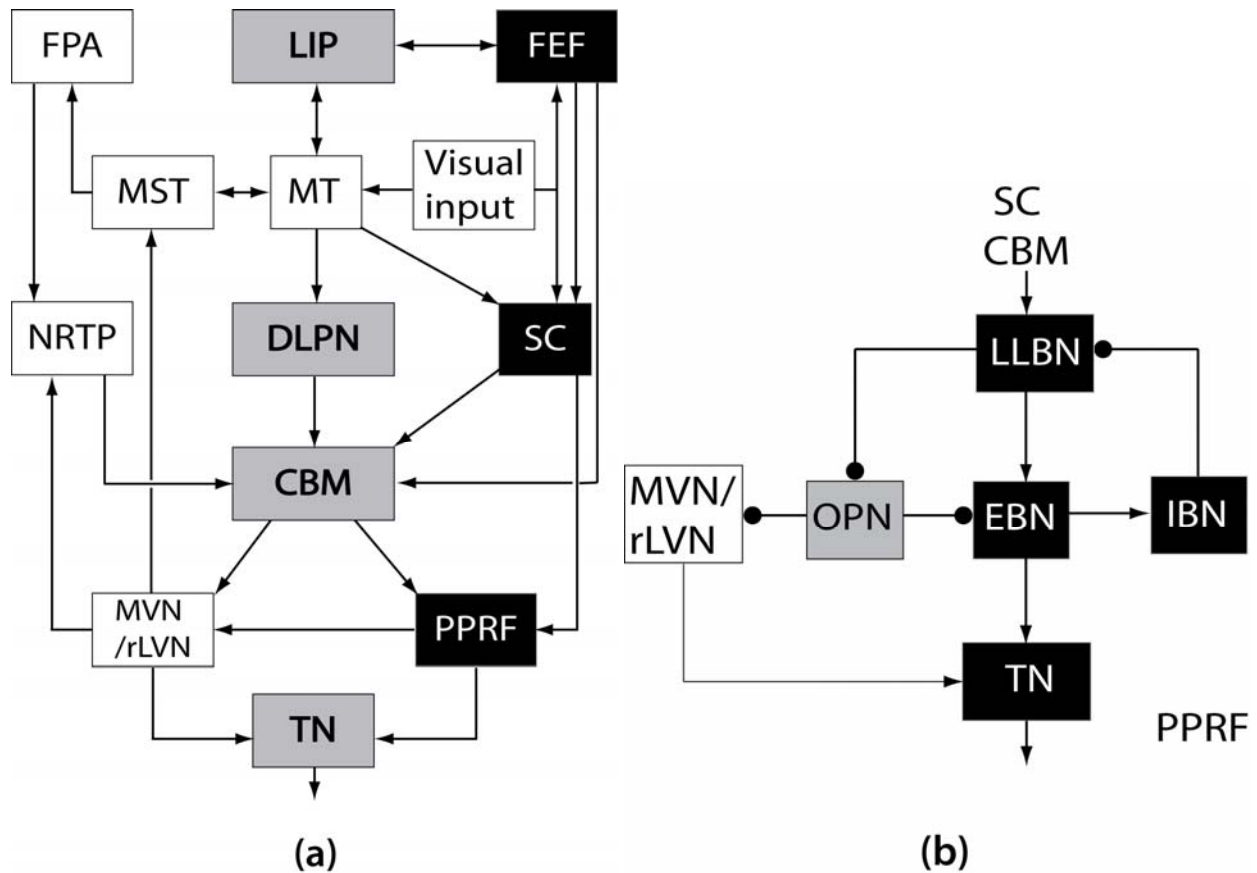


Figure 1: Modeled interactions among brain regions implicated in oculomotor control. In (a) black boxes denote areas belonging to the saccadic eye movement system (SAC), white boxes the smooth pursuit eye-movement system (SPEM), and gray boxes, both systems. LIP – Lateral Intra-Parietal area; FPA – Frontal Pursuit Area; MST – Middle Superior Temporal area; MT – Middle Temporal area; FEF – Frontal Eye Fields; NRTP – Nucleus Reticularis Tegmenti Pontis; DLPN - Dorso-Lateral Pontine Nuclei; SC - Superior Colliculus; CBM – cerebellum; MVN/rLVN – Medial and Rostro-Lateral Vestibular Nuclei; PPRF – a Peri-Pontine Reticular Formation; TN – Tonic Neurons. (b) Constituents of the saccade generator in the PPRF, and the projection of omnipause neurons to the pursuit neurons of the MVN/rLVN. Arrowheads terminate excitatory connections, and

circles terminate inhibitory connections. OPN - Omni-Pauser Neurons; LLBN – Long-Lead Burst Neuron; EBN- Excitatory Burst Neuron; IBN – Inhibitory Burst Neuron; TN - Tonic Neurons.

Model Overview

The model (Figure 1) consists of two parallel yet interacting processing streams for the control of SPEM and SAC movements. Neuroanatomy-based models of SPEM and SAC eye movements were used as starting points for this work: the SACCART model of learning and performance using a multi-modal movement map in the superior colliculus (SC; Gancarz & Grossberg, 1999; Grossberg, Roberts, Aguilar, & Bullock, 1997), the TELOS model of learned cue-guided voluntary selection of saccade plans (Brown, Bullock, & Grossberg, 2004), and a model of motion perception and SPEM command genesis in MST (Pack, Grossberg, & Mingolla, 2001). A complete mathematical specification of the model, and details regarding simulations, are provided in the Supplementary Material section.

The SPEM stream. Figure 1a gives an overview of the structure of the model SPEM circuit. The model's smooth pursuit stream contains visual area MT-like cell-types, which are distinguished by selectivity for different combinations of the direction and speed of visual stimuli that fall within their retinotopic receptive fields (Albright, 1984; Maunsell & van Essen, 1983a). The 800 model MT cells provide inputs to the model's MST cells, which pool their MT inputs in a way that makes them direction-selective and speed-sensitive, but not speed-selective. Because these MST cells also receive inputs corresponding to current eye velocity, they can compute an internal estimate of predicted target velocity that remains accurate even as eye velocity grows to match target velocity, and thus gradually cancels the target-related retinal image motion that drives MT cells.

The predictive estimate of target velocity computed by model MST cells provides a basis for the model's frontal cortical representation of desired pursuit velocity. In particular, the frontal pursuit area (FPA), at the rostral bank of the arcuate sulcus, receives inputs from both MST and MT (Huerta, Krubitzer, & Kaas, 1987; Tian & Lynch, 1996a, 1996b). Model and real FPA cells have high direction-selectivity and speed-sensitivity, but almost no speed-selectivity (Gottlieb, Bruce, & MacAvoy, 1993; Tanaka & Lisberger, 2002b).

The model FPA cells project (Brodal, 1980; Giolli et al., 2001) to the model nucleus reticularis tegmenti pontis (NRTP) which includes two types of cells: acceleration cells and velocity cells (Ono, Das, Economides, & Mustari, 2005; Ono, Das, & Mustari, 2004; Suzuki, Yamada, Hoedema, & Yee, 1999; Yamada, Suzuki, & Yee, 1996). Model NRTP velocity cells integrate the output of NRTP acceleration cells. The latter compute the difference between an excitatory target-velocity command from FPA and an inhibitory eye-velocity signal from the vestibular nuclei. This difference estimates the eye acceleration that is needed to match target velocity. These two classes of cells allow the NRTP to play a key role in SPEM initiation.

One possible source of this inhibitory eye velocity signal to NRTP might be from the ventrolateral thalamus. Neurons in ventrolateral thalamus discharged before or during initiation of pursuit, and the firing rate was proportional to the speed of target motion in a preferred direction. When the tracking target was extinguished briefly during maintenance of pursuit, these neurons continued firing, indicating that they carried extraretinal eye movement signals (Tanaka, 2005).

Parallel to the FPA-NRTP pathway, a second pathway exists for the transmission of SPEM-related information from the cortex to the cerebellum via the pons. This pathway, apart

from being implicated in maintenance of SPEM (Mustari, Fuchs, & Wallman, 1988; Suzuki & Keller, 1984), also helps to program saccades made to moving objects. Model MT cells project to dorsal lateral pontine nucleus (DLPN) cells of the brain stem which then project to cerebellum (Figure 1a). In the model, the DLPN cells have similar speed and directional selectivities as MT cells, but they lack their retinotopic specificity.

The SAC stream. In the model saccadic system, retinotopically organized visual signals are processed to produce saccadic target choices in the model lateral intra-parietal area (LIP) and frontal eye fields (FEF). FEF outputs serve as inputs to corresponding retinotopic loci in the burst and buildup cell layers (Munoz & Wurtz, 1995a, 1995b; Sommer & Wurtz, 2000, 2004) of the motor error map of the model's superior colliculus (SC). There is also communication between these SC layers, such that activated loci in the burst cell layer excite corresponding cells in the buildup cell layer (cf. Grossberg et al., 1997).

Outputs from the SC reach the cerebellum and the saccade generator circuit (Figure 1b) in the para-median pontine reticular formation (PPRF), which contains populations of SAC- and SPEM-related cells, some of which provide direct input to the oculomotor neurons that innervate eye muscles. Model saccadic control signals from cerebellar and SC stages converge at model long lead burst neurons (LLBN). LLBN activity encodes gaze-position error. LLBN cells excite corresponding excitatory burst neurons (EBN), which project to the tonic neurons (TN). TNs integrate inputs from EBNs and excite the model oculomotor neurons. The EBNs also excite inhibitory burst neurons (IBN), which in turn inhibit the LLBNs, thereby completing an internal negative feedback loop that controls ballistic saccades. Except during saccades, the EBNs receive strong inhibition from model omni-pause neurons (OPNs), so-called because they pause deeply to disinhibit saccades of all directions. For reviews of these anatomical connections and neurophysiological properties, see Buttner and Buttner-Ennever (1988, 2005), Fuchs et al. (1985), and Moschovakis and Highstein (1994). For reviews of computational models that incorporate such features, see Girad & Berthaz (2005).

Shared omni-pausers. OPNs are located in the nucleus raphe interpositus. The pursuit neurons (PNs) found in the vestibular nuclei are modeled as receiving input from the cerebellum and projecting directly to the TNs, which are thus shared by SAC and SPEM systems. The PNs are weakly inhibited by, and themselves inhibit, the OPNs, also shared by both systems. About 50% of the OPNs show reduced activity (a 34% drop) during smooth pursuit (Missal & Keller, 2002), whereas most OPNs pause more deeply during saccades (Everling, Pare, Dorris, & Munoz, 1998; Munoz, Dorris, Pare, & Everling, 2000). Thus, the spontaneously active and inhibitory OPNs normally oppose both saccades and SPEM. Shallow pausing by OPNs can release SPEM but not saccades, whose release requires deeper pauses.

Cerebellar learning calibrates SPEM and SAC commands. Learning is needed to keep SAC and SPEM metrics accurate as eye muscles and other system parameters change. Inactivation or lesion of the cerebellum causes deficits in the ability to adapt both saccadic and smooth pursuit eye movements (Takagi, Zee, & Tamargo, 1998). Each model cell in the retinotopic SC, the speed-sensitive DLPN, and the direction-sensitive NRTP sends signals to the cerebellum (Thier & Ilg, 2005). These signals are modified by adaptive weights learned within the cerebellum. The adaptive saccade-related cerebellar outputs reach the model para-median pontine reticular formation (PPRF) region of the brain stem (Figure 1a), the location of the saccade generator (Figure 1b). Similarly, the weighed pursuit-related cerebellar outputs reach the pursuit neurons (PNs) in the vestibular nuclei of the brain stem.

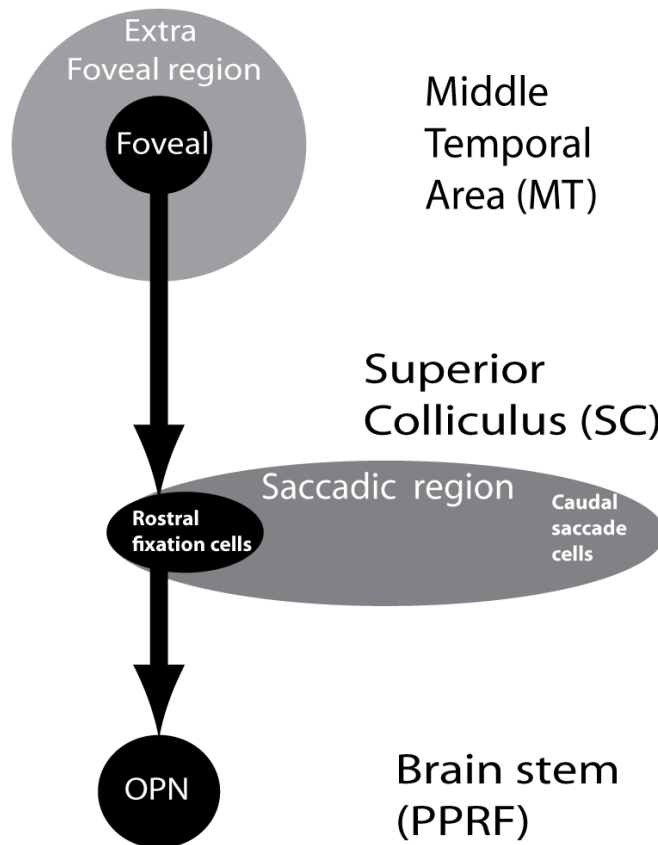


Figure 2: Cortico-colliculo-reticular control of saccade initiation. The figure illustrates a pathway from foveal and para-foveal cells in cortical area MT to the rostral pole of the SC and then to the OPNs in the PPRF. In the model, effective tracking causes MT foveal cells to become active. This, in turn, activates fixation cells present in the rostral SC. Such SC cells excite OPNs, which can inhibit saccade initiation or suspend on-going saccades.

SPEM system inhibition of SAC initiation via an MT - SC - OPN pathway. Behavioral data (simulated in Grossberg et al., 2007) suggest the existence of an intelligent mechanism to control saccade initiations during SPEM, notably to inhibit saccades when targets are already foveal or parafoveal. Pursuit-related neural activity is reliably observed in the SC: Rostral parts of SC (rSC) contain cells that respond to both SPEM and saccadic eye movements (Krauzlis, Basso, & Wurtz, 2000). As schematized in Figure 2, area MT sends strong excitatory projections to the rostral part of SC (rSC) (Collins, Lyon, & Kaas, 2005; Davidson & Bender, 1991; Maioli, Domeniconi, Squatrito, & Riva Sanseverino, 1992; Spatz & Tigges, 1973; Wall, Symmonds and Kaas, 1982), which in turn provides the main excitatory input to the OPNs (Everling et al., 1998; Gandhi & Keller, 1997; Pare & Guitton, 1994). Our hypothesis that rSc projects to the OPN is consistent with data from Buttner-Ennever et al. (1999) which state that “there are multiple projections directly onto OPNs from the rostral SC but not from the caudal SC associated with large gaze shifts...”. Also, the place where FEF fibers terminate appears identical to the region where SC fibers terminate (Buttner & Buttner-Ennever, 1988). Stanton et al. (1988) found direct projections from the fundus of the arcuate sulcus (FEF) to a region in nucleus raphe (OPNs) identical to where SC fibers terminate. So, we hypothesize that OPNs might be getting foveal input from both FEF and SC. In the model (Figures 1 and 2), foveal and

para-foveal cells in area MT, which are active when pursued targets are on or near the fovea, inhibit saccades via an excitatory pathway from MT to rSC to the OPNs.

Target selection in the two streams. Selecting a saccadic target present among competing distracters, as in a visual search paradigm (Treisman & Gormican, 1988), requires dissociation of target stimuli from others. Visually responsive neurons in the frontal eye fields (FEF) show this discrimination. Late phase activity of these neurons was accentuated for targets and attenuated for distracters that excited their motor receptive fields (Schall, Hanes, Thompson, & King, 1995; Schall & Thompson, 1999; Thompson, Bichot, & Schall, 1997; Thompson, Hanes, Bichot, & Schall, 1996). Stimulation of a LIP, FEF or SC neuron increases the probability of choosing the stimulus within its motor field as the target (Carello & Krauzlis, 2004; Schiller & Tehovnik, 2001, 2003), and reversible inactivation of FEF, LIP, and SC produces significant saccadic target selection deficits (McPeck & Keller, 2004; Schiller & Tehovnik, 2003; Wardak, Olivier, & Duhamel, 2002).

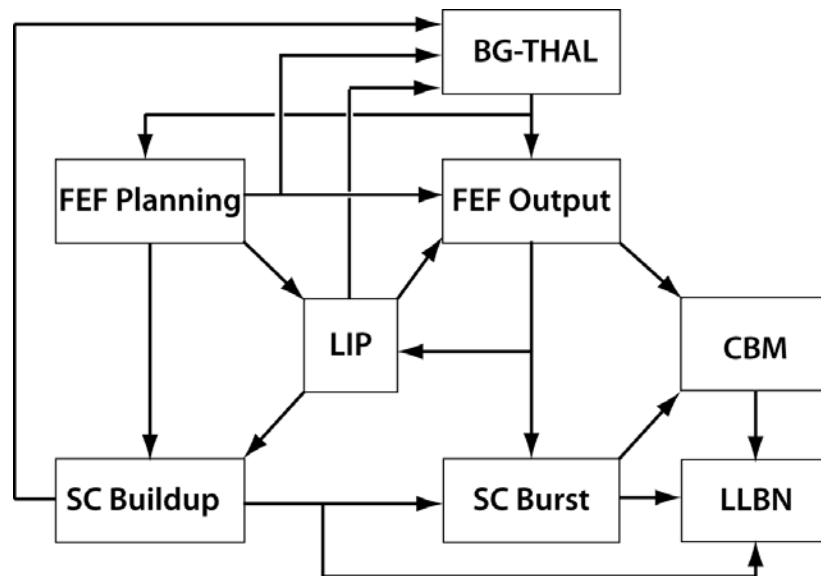


Figure 3: Fronto-parietal circuit interactions leading to target selection. The figure shows connections in the model's SAC pathway that help choose a target among competing stimuli. FEF planning neurons, LIP neurons, and SC buildup neurons send collaterals to a decision stage representing the basal ganglia and thalamus (BG- Thalamus). Once a BG- Thalamus (BG- Thalamus) decision is made regarding the choice of target, a GO signal is sent from thalamus to FEF planning and output neurons. The signal from thalamus boosts the activity of all cells in the corresponding part of FEF. With the help of the GO signal and mutual inhibition, network interactions amplify a weak initial advantage by one planning cell into a winner-take-all choice of that planning cell and its corresponding output cell. The Figure also shows that the target selection decision is transmitted from FEF output cells via SC and CBM to LLBNs in the saccade generator (in PPRF; see also Figure 1).

In the model, interactions in the parieto-frontal circuit (LIP-FEF-LIP) are critical for selecting targets among competing distracters. Figure 3 schematizes interactions in the SAC pathway that lead to target selection. FEF planning neurons (similar to the FEF visual motor cells in Schall, Hanes, Thompson, & King, 1995), which receive input from lower level visual areas (not

shown), send outputs to LIP, FEF output neurons (similar to the FEF motor cells in Schall, Hanes, Thompson, & King, 1995), SC buildup neurons, and the striatum of the basal ganglia (Schall, Morel, King, & Bullier, 1995). In amphibians and all land vertebrates, the basal ganglia (BG) interact with the optic tectum (OT), or its homolog, the SC, to control orienting action (Butler & Hodos, 1996; Marin, Smeets & Gonzalez, 1998). In mammals, the BG interact with frontal cortical areas to control orienting, cognitive, and manipulative behaviors (Hikosaka & Wurtz, 1989; Passingham, 1993; Strick, Dum & Picard, 1995). Lesions of the BG cause disorders such as Parkinsonian akinesia, Huntington's chorea, and ballism (Albin, Young & Penney, 1989), suggesting a strong link between BG and areas involved in movement control. These interactions provide a natural basis for differentiating plan activation and plan execution. Brown et al. (2004) developed a detailed neural model of how FEF and BG interact with movement-controlling areas such as SC.

The current SAC-SPEM model approximates BG-mediated decision-making by sending a *GO signal* excitation to FEF if the sum of the FEF, LIP and SC signals associated with a particular saccadic vector is large enough to exceed a threshold. *In vivo*, this signal results from striatal disinhibition of the thalamus, and can be regarded as opening a normally closed gate to release the planned movement (Brown et al., 2004; Lo & Wang, 2006; Wurtz & Hikosaka, 1986). Once the gate is open, the FEF cell having maximal activity is selected as the target, and it suppresses other target representations via mutual inhibition.

We predict that the smooth eye movement part of the frontal eye fields, known as the frontal pursuit area (FPA), is involved in decision-making for SPEM and for coordinated tracking by SPEM and SAC. The FPA, located near the rostral bank of the arcuate sulcus, is strongly innervated by MST (Huerta et al., 1987; Tian & Lynch, 1996a, 1996b). FPA cells have high direction-tuning and almost no speed-selectivity (Gottlieb et al., 1993; Lynch & Tian, 2005; Tian & Lynch, 1997; Tian & Lynch, 1996a, 1996b). Lesions in FPA cause SPEM deficits, including reduction of pursuit gain and directional deficits (Keating, Pierre, & Chopra, 1996; Shi, Friedman, & Bruce, 1998). Electrical stimulation of FPA causes SPEM, and, if applied during natural SPEM, such stimulation increases SPEM gain if the natural pursuit direction and the stimulated direction are the same (Carey & Lisberger, 2004; Gottlieb et al., 1993; Tanaka & Lisberger, 2002a, 2002b, 2002c).

In the model, a SPEM target choice can be made independently by the FPA under the influence of visual motion inputs from MT and MST. Directions of all the moving objects in the environment form retinotopically organized peaks of activity of neuronal populations in MT. We hypothesize that FPA, which lies downstream from MT and MST, converts this sensory signal to a motor signal for movement. This assumption is in agreement with data showing multiple peaks in MT, before selection occurs downstream (Treue et al., 2000). This fact is reflected in model dynamics (compare Figures 7e and 7f below). Related data about selection of saccadic movement commands beyond MT can be found in Roitman & Shadlen (2002) and Shadlen & Newsome (2001), and are modeled in Grossberg & Pilly (2008).

A GO signal that represents the excitatory thalamocortical output of the BG-thalamus system is released when the FPA signal to the BG exceeds a threshold for movement initiation. This assumption accords with recent data (Cui, Yan, & Lynch, 2003) indicating that the FPA connects with the BG-thalamus system in a way that parallels FEF connections with that system (see Brown et al., 2004).

Although both SAC and SPEM systems can reach decisions, the model also provides for coordination. Krauzlis et al. (1999) found that once a target has been selected by the saccadic

system, and a saccade initiated, it is rare for the eye to move along the direction of any contending stimulus after the saccade. Figure 1a shows that there is a path in the model (and in vivo) from FEF to LIP to MT to MST to FPA. This model pathway mediates transfer of the SAC system's target choice to the SPEM system. This transfer enables the SAC system to override the SPEM system. Although, FEF and FPA are nearby in frontal cortex, the model links them via other areas, and not directly, in accord with both computational and anatomical constraints.

The LIP is key in that linkage. First, it receives collaterals from both saccadic and smooth pursuit pathways (Maunsell and Van Essen, 1983; Schall et al., 1995b; Tian and Lynch, 1996a, 1996b). Second, its activity strongly reflects a monkey's decision about a subsequent eye movement, and choice-related up-modulation of direction-tuned cells are seen regardless of whether the sensory inputs driving this decision are stationary or moving stimuli (Gold & Shadlen, 2000, 2001; Schiller & Tehovnik, 2005; Shadlen & Newsome, 2001). Grossberg and Pilly (2007) describe a model for how motion stimuli influence LIP decision making. Third, activation of LIP affects target choice without affecting the saccade metrics like saccade duration or velocity (Schiller & Chou, 1998; Schiller & Tehovnik, 2005; Thomas & Pare, 2007; Wardak et al., 2002).

Results: Comparisons of Simulations with Data

The Supplementary Material section provides simulation details, including the system of differential equations that, together with external inputs, govern the model circuit's dynamics.

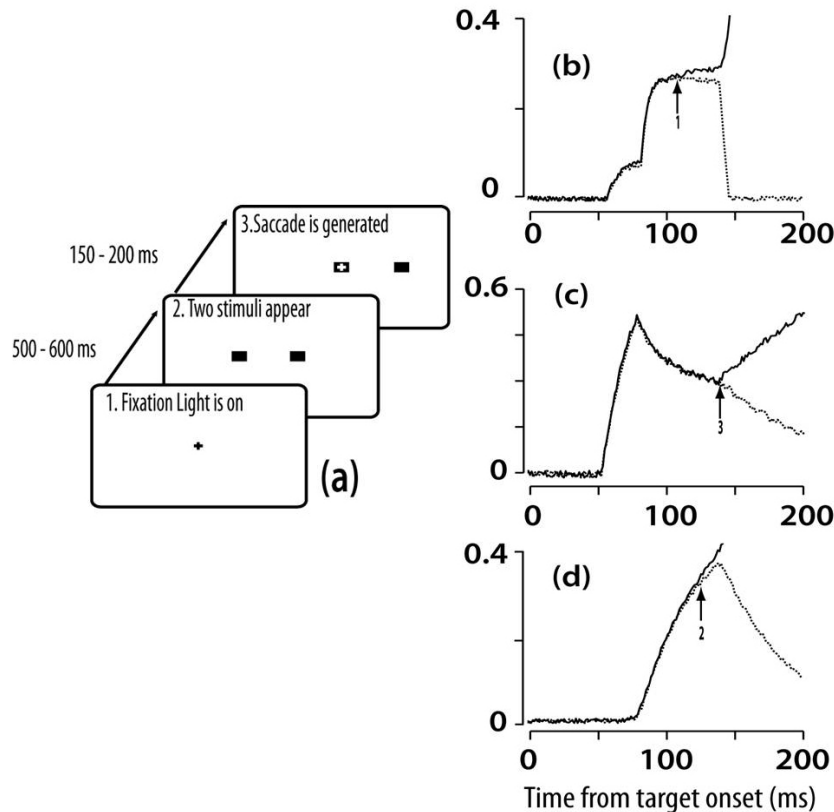


Figure 4: Saccadic target selection: Paradigm and simulations. Panel (a) schematizes the paradigm used to simulate saccadic target selection. Two similar stimuli are flashed on

either side of, and at the same eccentricity from, a central fixation point. After 150-200 ms, the model generates a saccade that brings the fovea onto whichever of the two stimuli was selected as the target. Panels **(b)** to **(d)** illustrate how this selection is achieved by the model. In each panel, a dotted trace shows the activity of the neuron with the distractor (non-chosen stimulus) in its RF, whereas the thick trace shows the activity of a neurons with the target in its RF. Panel **(b)** shows the activities of two FEF planning neurons, panel **(c)** shows two LIP neurons and panel **(d)** shows activities of FEF output (presaccadic burst) neurons. During the initial 100ms after stimulus presentation, the activities evolve similarly for each pair. Around 120 ms, a small separation opens between the competing neuron types in FEF (arrows 1 and 2), but not in LIP. Around 140 ms, the activity (not shown) of the BG-Thalamus decision process reaches its threshold and a GO signal is generated. This is followed immediately by rapid growth in FEF activations for the target and rapid suppression of FEF activations for the distractor. This choice induces a similar choice in LIP (arrow 3, in **d**).

Simulation 1. Simulating how voluntary choice of a saccadic eye movement target is made by interactions among frontal, subcortical, and parietal areas. Consider the case of selecting a saccadic target among two stimuli (see Figure 4a). The initial phase of activity (50 – 100 ms) is similar for both target and distractor (see Figure 4b, 4c & 4d), consistent with observations that visual neurons of the FEF show transient activity as early as 50 ms after stimulus onset (Schall, Hanes et al., 1995). But the second phase of activity is selective for the target. FEF planning neurons representing the target increase, and other neurons representing distractors decrease, in their activity (Figure 4b). Since the two stimuli are identical, there is an equal probability for either to be chosen as target. The choice is the result of a competitive race between the cells coding the two stimuli. Attentional bias, in the form of oddball size, shape or color stimulus can help break the symmetry and determine the winner. In the present case, no such bias was present, so noise was added at the FEF stage. After an interval of slow separation between the competing representations, which begins in FEF cells at the time marked by arrows 1 and 2 in Figures 4b and 4d, the BG-Thalamus stage reaches threshold. Its output (GO signal) to FEF initiates the rapid separation that is visible first in FEF planning and output cells (4b and 4c), and, after a brief delay, in LIP cells (Figure 4c, arrow 3). Thus the model predicts that the choice is made by the frontal circuit and rapidly relayed to LIP. Cortical lateral inhibition mediates the model's rapid suppression of the unchosen representation.

Figure 5 compares the simulated activity of model FEF planning and output neurons with FEF electrophysiological recordings (Schall et al., 1995) from a visual search experiment in which targets were clearly discriminable from distractors. In the simulation, this difference was mimicked by making one stimulus 1.5 times as strong as another one. The stronger stimulus was always chosen, and the activation profiles in the model are qualitatively similar to the recordings.

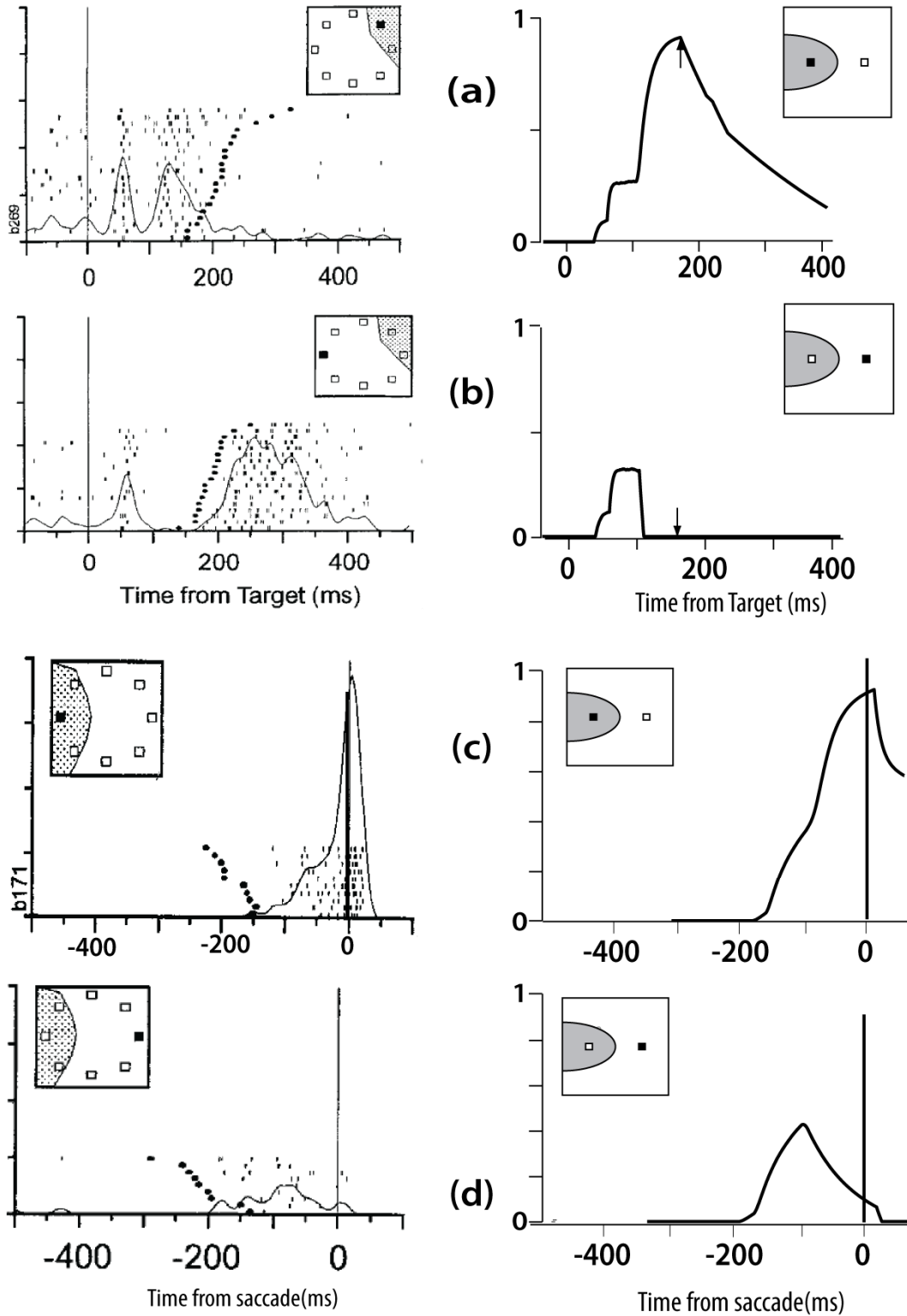


Figure 5: Role of FEF in target selection decisions: Data and simulations. The right column presents model FEF planning (a, b) and output (c, d) neuron activities for comparison with real (left column) visuomotor (a, b) and presaccadic/motor (c, d) neuron activities recorded during saccadic target selection in a visual search paradigm (J. D. Schall,

Hanes et al., 1995). Panels (a) and (c) depict activities of neurons representing to-be-foveated targets, while panels (b) and (d) depict activities of neurons representing distractors. The shaded areas in the box inserts (one in each panel) indicate the neurons' receptive fields. Targets are indicated by filled black squares, distractors by white squares. The small vertical arrows in panels (a) and (b) in the right column indicate the time of saccade initiation. For panels (a) and (b), time zero represents stimulus onset. For panels (c) and (d), time zero represents saccade onset.

Simulation 2. Simulating how voluntary choice of a smooth pursuit eye movement (SPEM) target is made by the frontal pursuit area (FPA). Often, one of several moving stimuli is chosen for tracking by SPEM, in the absence of any saccades. If two moving stimuli are nearby the initial gaze position, then the direction of this SPEM often begins as the vector average of the two stimulus motion directions, then quickly evolves into pursuit along the direction of one stimulus. The second phase reflects a decision, which is also signaled by an increase in SPEM gain: the ratio of eye velocity to target velocity (SPEM gain) is much lower during the initial vector averaging phase than after the system has committed to pursuit of one target. Figure 6 highlights the idea that the phase transition occurs once a decision process in the BG-Thalamus exceeds the threshold for generating a GO signal that increases the output from FPA averaging cells to subcortical SPEM generators.

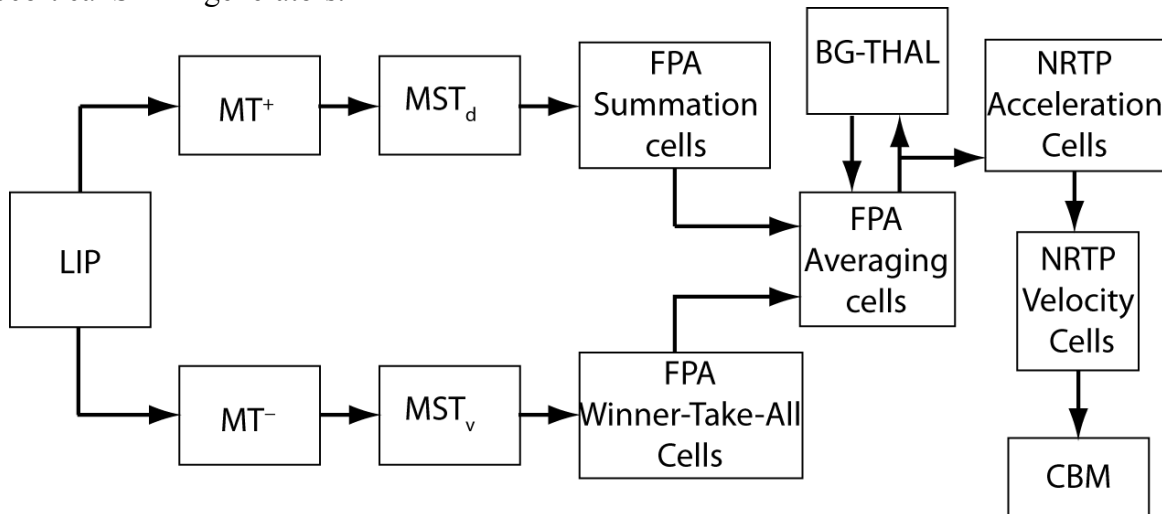


Figure 6: Model of visual motion and SPEM pathway. The Figure shows model cortical and sub-cortical connections along the visual motion and SPEM pathway. In addition to their visual input (see figure 1), MT+ and MT- receive input from LIP. The receptive fields of model LIP and MT are aligned retinotopically. MT- cells project to MSTv and MT+ cells project to MSTd. FPA input (FPAi) or WTA cells receives projections from MSTv cells and in turn projects to FPA output (FPAo) or averaging cells. FPAo cells also get input from MSTd cells via FPA summation (FPAs) cells. Strong mutual inhibition, and connections with a decision stage representing basal ganglia and thalamus (BG- Thalamus) help FPAo cells achieve target selection. This information is carried to cerebellum via acceleration and velocity cells of the NRTP.

Figure 7 presents simulation results that illustrate the model's ability to generate a similar transition between vector averaging and choice of one target for high-gain SPEM, and also shows the consequence of the decision for the activity of model FPA output cells. Unlike

saccadic vector averaging, which holds for an entire saccade, and occurs only when there is small angular separation between the potential targets and when SAC latency is very short (Arai, McPeck, & Keller, 2004; Ottes, Van Gisbergen, & Eggemont, 1984), pursuit averaging is more commonly observed (Gardner & Lisberger, 2001, 2002; Recanzone & Wurtz, 1999; Tanaka & Lisberger, 2002c). In the model, the difference between the two systems occurs because the output cells in FPA can become partly activated before a decision is reached, unlike output cells of FEF. Such a lower threshold for output from FPA than FEF makes behavioral sense, because averaging low-gain SPEM incurs no visual cost, whereas a premature saccade would impose costs in the form of an interval of reduced vision and de-foveation of the target.

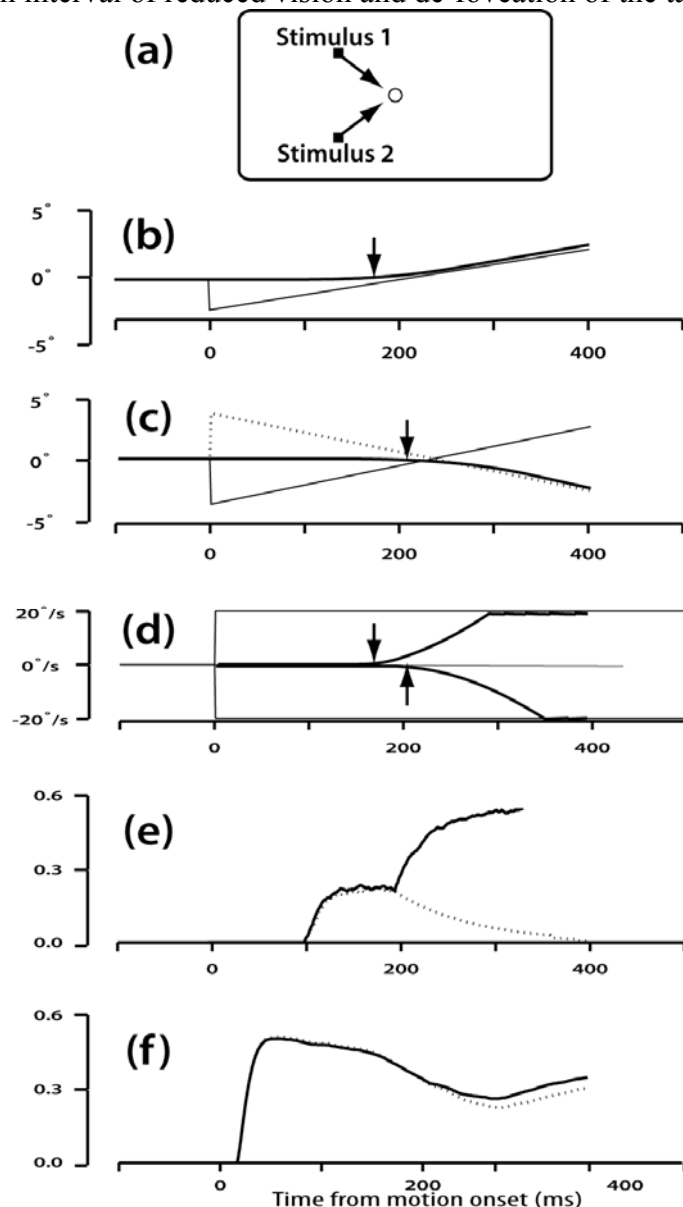
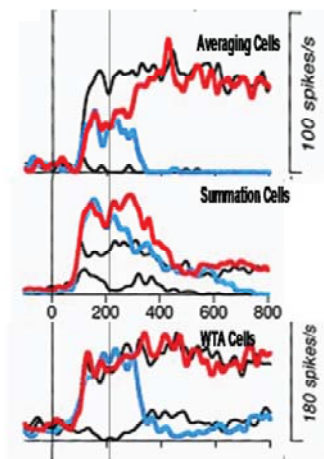


Figure 7: Simulated smooth pursuit target selection for two stimuli that are moving towards each other. The Figure illustrates how activities of various cells help decide a target for SPEM. The paradigm used is a modified double target paradigm. The initial unsigned speeds of the two stimuli are the same, and the position-speed combinations are such that no saccade is needed to initiate tracking of either of the two stimuli. In panel (a), *Stimulus 1*

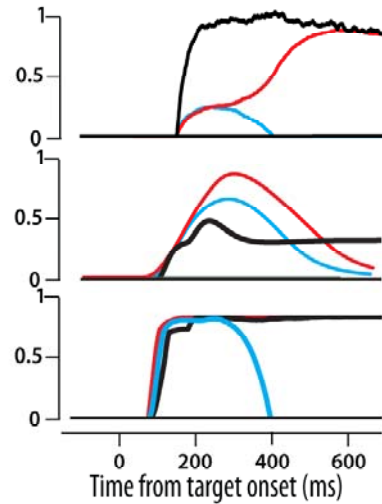
starts at $[-4^\circ \text{ H}, -5^\circ \text{ V}]$ and moves at $20^\circ/\text{s}$ along the 45° direction; *Stimulus 2* starts at $[-4^\circ \text{ H}, 5^\circ \text{ V}]$ and moves with a speed of $20^\circ/\text{s}$ along the 305° direction. Panel (b) shows the horizontal and (c) the vertical eye position components, and the corresponding two components of the two stimuli's positions. In both panels (b) and (c), the thin black line is the trace of the stimulus selected as target and the thin dotted line represents the trace of the distractor. The thick black line represents the eye trace. Arrows in the panels represent the time at which the eye moves along that particular axis (i.e. panel (b) shows the time at which the eye moves in the horizontal direction and the arrow in panel (c) indicates the time at which the eye moves in the vertical direction). Since the two stimuli move in oblique directions, the eye moves along the vector-averaged direction (rightward direction here) before making a target choice decision; this is evident from the arrow positions in panels (b), (c) and (d). Panel (d) shows the horizontal and vertical eye and target velocity traces. The thick black trace rising in the positive (upward) direction shows the horizontal eye velocity component and the thin dotted trace dropping in the negative direction shows the later-starting vertical component of eye velocity. These component velocities asymptote at the target velocity components, $20^\circ/\text{s}$ H and $20^\circ/\text{s}$ V. Panels (e) and (f) illustrate the crucial SPEM model activities enabling choice. Panel (e) shows activities of two FPA output ("averaging") cells (see Figure 6). And panel (f) illustrates the activities of MSTv cells. Thick black lines in both panels ((e) and (f)) show the activity trace of the cell whose preferred direction was along the direction of motion of the stimulus selected as target and the thin dotted line represents the activity trace of the cell whose preferred direction was along the direction of motion of the distractor. At around 150 ms, FPA cells show early signs of target selectivity. Between 150 to 200 ms, vector averaging takes place as the FPA contains representations of both target and distractor. FPA output neurons project to a decision stage conceptualized as a BG-Thalamus stage partly analogous to that in the SAC system. At around 190 ms, the decision stage activity reaches a threshold and generates a GO signal to FPA. This boosts the activity of the cell with maximal activity, causing it to be selected.

Figure 6 shows that two further classes of model FPA cells, which correspond to what Tanaka and Lisberger (2002c) called "summation" and "WTA" (winner-take-all) cells, receive inputs from model areas MST_d and MST_v , respectively, and excite FPA output (averaging) cells. Figure 8a shows data on all three types of FPA cells, and Figure 8b shows how the model simulates the qualitative differences between these cell-types under the three conditions tested. These patterns illustrate that both summation cells and WTA cells come close to their maximum activities levels during the vector averaging phase; i.e., before a choice has been made, whereas the output (averaging) cells show much lower than maximal activity until the disappearance of one target results in choosing the one that remains. This property suggests that the averaging cells are output cells that reflect the BG-Thalamus decision process.

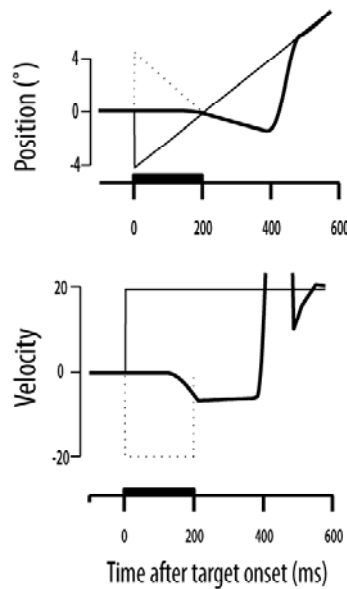
Note that summation cells show a decline in activation during SPEM maintenance (in the latter part of the trial), whereas WTA cells show sustained activity during this interval. This difference is explicable in the model because summation cells receive input from area MST_d cells, which become much less active as successful SPEM cancels target motion signals in the retinal frame, and because WTA cells receive inputs from MST_v cells, which remain active even during successful pursuit because they receive a corollary discharge of eye velocity (Pack et al., 2001).



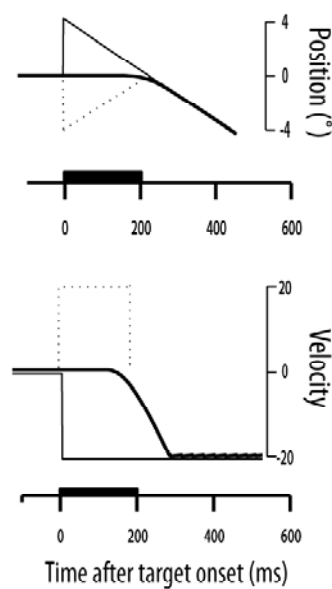
(a)



(b)



(c)



(d)

Figure 8: Simulated effect of FPA stimulation on smooth pursuit target selection. Panel (a) shows the measured activities of three types of cells found in FPA (M. Tanaka & Lisberger, 2002c). A double-target and a single-target paradigm were used. In the former, two stimuli appeared at the same time at 4° eccentricity on either side of the fixation point. They start moving towards each other at $20^\circ/s$, and at 200 ms, which coincides with the time their trajectories cross, one of the stimuli is extinguished. The remaining stimulus should be selected as target and tracked. In the single-target paradigm, a single target appeared at 4° eccentricity and started moving towards the fixation point at $20^\circ/s$. The eccentricities and velocities were set so as not to elicit any saccades. In each column, the color of the neuron

activity trace codes the condition under which the activity was recorded. *Red Trace*: double-target paradigm, with the remaining target's motion in the direction preferred by the neuron; *Blue trace*: double-target paradigm, with the remaining target's motion in the direction opposite to that preferred by the neuron. The black traces are activities from single-target control trials, in which target motion matched the cell's preferred direction. Panel (b) shows simulations of activities of the corresponding three types of model cells, in the same paradigms. The top row in (a) and (b) shows "averaging" or "output" cells, the middle row shows "summation" cells, and the bottom row shows "winner-take-all" or "input" cells. Panels (c) and (d) show simulation results when the model FPA was stimulated during SPEM target selection. The paradigm used was the double-target paradigm described above. The thick black bar on the x-axis in each panel represents the interval (0-200 ms) during which a left-motion-tuned model FPA output cell was stimulated. In both panels (c) and (d), thin black and thin dotted black lines represent the kinematic traces of two stimuli. The thin black line is the trace of the stimulus selected as target, the dotted line that of the distractor. The thick black trace represents the trace of the eye through time. The top rows in panels (c) and (d) represent target and eye position traces. The bottom rows represent the stimuli and eye velocity traces. The left column (c) shows the case when the leftward (plotted as downward) moving stimulus was extinguished after 200 ms. The right column (d) shows the case when the rightward-moving (plotted as upward) stimulus was extinguished. In panel (d), the model continues to track the artificial-stimulation-selected target, which remains visible. In panel (c), the target initially selected for SPEM tracking by artificial FPA stimulation in the model is abandoned once the stimulation ceases and the target stimulus disappears. The model takes around 200 ms to generate a catch-up saccade (at around $t=400$ ms) to the rightward-moving target, after which the eye smoothly tracks it.

If FPA is involved in deciding which stimulus to follow, then stimulation of FPA should bias the result during target selection. Since microstimulation in FPA causes eye movements along the particular direction represented at the stimulation site, any stimulus moving along this direction should be favored and selected over competing stimuli. Data of Tanaka and Lisberger (2002c, Figure 6) confirm this idea. The simulation results plotted in Figure 8c and 8d show that this is also true of the model. Initially, there are two stimuli moving in opposite directions (left and right directions in our simulations) and towards the fixation point. Selective stimulation of left-tuned model FPA output cells causes leftward (plotted as downward) SPEM. At 200 ms after the stimulus onsets, one of the stimuli disappears (in Figure 8c, the left-moving stimulus disappears; in Figure 8d, the right-moving stimulus disappears). At the same time, the stimulation to FPA ceases. Figure 8c exemplifies a case in which the stimulated direction does not match that of the target that remains after stimulation offset. Following stimulation offset, the eye stops moving leftward, makes a rightward catch-up saccade, and then pursues the right-moving target. Figure 8d illustrates what happens when the electrically stimulated direction is the same as the direction of the remaining target. Although the SPEM latency is the same for stimulation and non-stimulation cases, the eye reaches target velocity faster when the FPA is stimulated.

Simulation 3: Simulating how pursuit initiation is altered by a moving distractor. The latency of SPEM initiation depends on the distribution of directions of moving stimuli. Adding a second moving stimulus will increase or decrease the latency of SPEM initiation if the second stimulus moves, respectively, in the same or the opposite direction as the chosen target (Ferrera & Lisberger, 1995). Note that in the case of oppositely moving stimuli, the vector average will

be no movement. In such cases, no SPEM will be observed until the system truly makes a choice. In the model, stimuli moving in different directions activate cells in MT and MST that are tuned to these directions. Such direction-sensitive cells project to cerebellum (CBM) and later output stages via two pathways (Figure 1a): one via dorso-lateral pontine nuclei (DLPN) and another via FPA and nucleus reticularis tegmenti ponti (NRTP). Although both branches can contribute to short-latency SPEM via vector averaging, neither will do so when the average of two opposing motions is zero. But if two potential targets are moving in the same direction, MT, MST and FPA summation cells coding this direction will often be more active, notably if there are two motion inputs within their receptive fields. The summation cells of FPA almost double their firing rate (Figure 8a, middle panel) if they contain two targets in their receptive field. This leads to faster activation of FPA output cells. Faster activation of FPA output cells leads to faster CBM cell activation and thus to faster pursuit initiation. Figure 9 illustrates these effects, and shows model simulations (right) next to behavioral data (Ferrera & Lisberger, 1995).

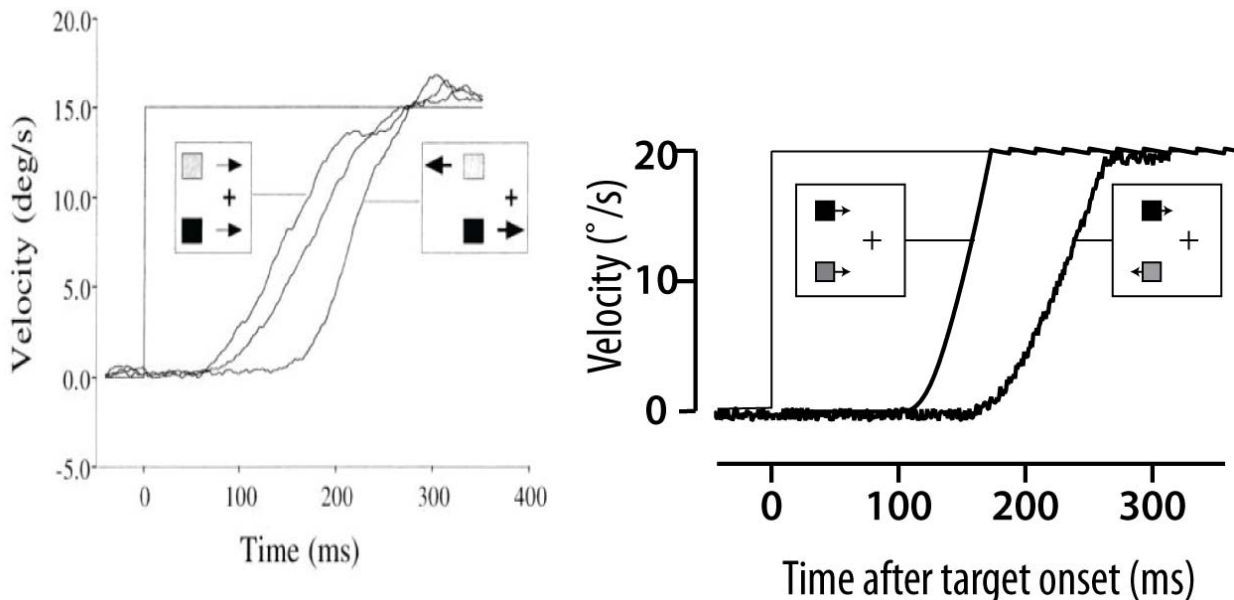


Figure 9: Effect of distractor direction on latency of smooth pursuit initiation. The Figure shows how the direction of a distractor affects the latency of SPEM initiation. The paradigm simulated was a modified double-stimulus paradigm. Two stimuli were flashed at the same time, on the same side, and at the same eccentricity, relative to the fixation point, but vertically displaced from each other. They start moving horizontally, either in the same or in opposite directions. The Figure compares model eye velocities with the data (reprinted, with permission, from Ferrera and Lisberger, 1995) during the first 300 ms of tracking. In data and model, when the direction of motion of the distractor (grey box in right column) matches that of the target (black box in right column), SPEM is initiated earlier than if the motion directions mismatch. This is seen in the trace offsets in both the right (model) and left (data) columns.

Simulation 4: Simulating how saccadic target choice overrides the choice made by smooth pursuit. Behavioral and neurophysiological data indicate that target selection can occur independently in the SAC and SPEM sub-systems, as simulated above. Independent selection raises a coordination problem: Which choice dominates in a tracking episode, and how is the

coordination achieved? We hypothesize that SAC choice overrides SPEM choice. Data from behavioral (Adler et al., 2002) and microstimulation (Gardner and Lisberger, 2001, 2002) experiments support this claim. Figure 10 compares model simulations (right) of the Gardner and Lisberger (2002) paradigm with their published data (left). In this double-stimulus paradigm, where natural saccades to either stimulus are equiprobable, an FEF site with a known directional preference and movement receptive field is stimulated after pursuit initiation, just as one stimulus enters the movement field, but before any natural saccades would occur. The stimulation evokes a saccade to the stimulus, even if the pre-saccadic SPEM was tracking the other stimulus. Moreover, SPEM velocity after the evoked saccade almost always matches the velocity of the saccadic target, not the velocity of the stimulus being tracked before the evoked saccade. Thus, SAC choice overrides an existing SPEM choice. In the model, these properties emerge because focal FEF stimulation activates a corresponding retinotopic zone in LIP, which in turn activates a retinotopic zone in MT and MST, within which inputs from the motion of the favored target will activate the correct direction-tuned cells that project to later stages of the SPEM system (Figures 1 and 6).

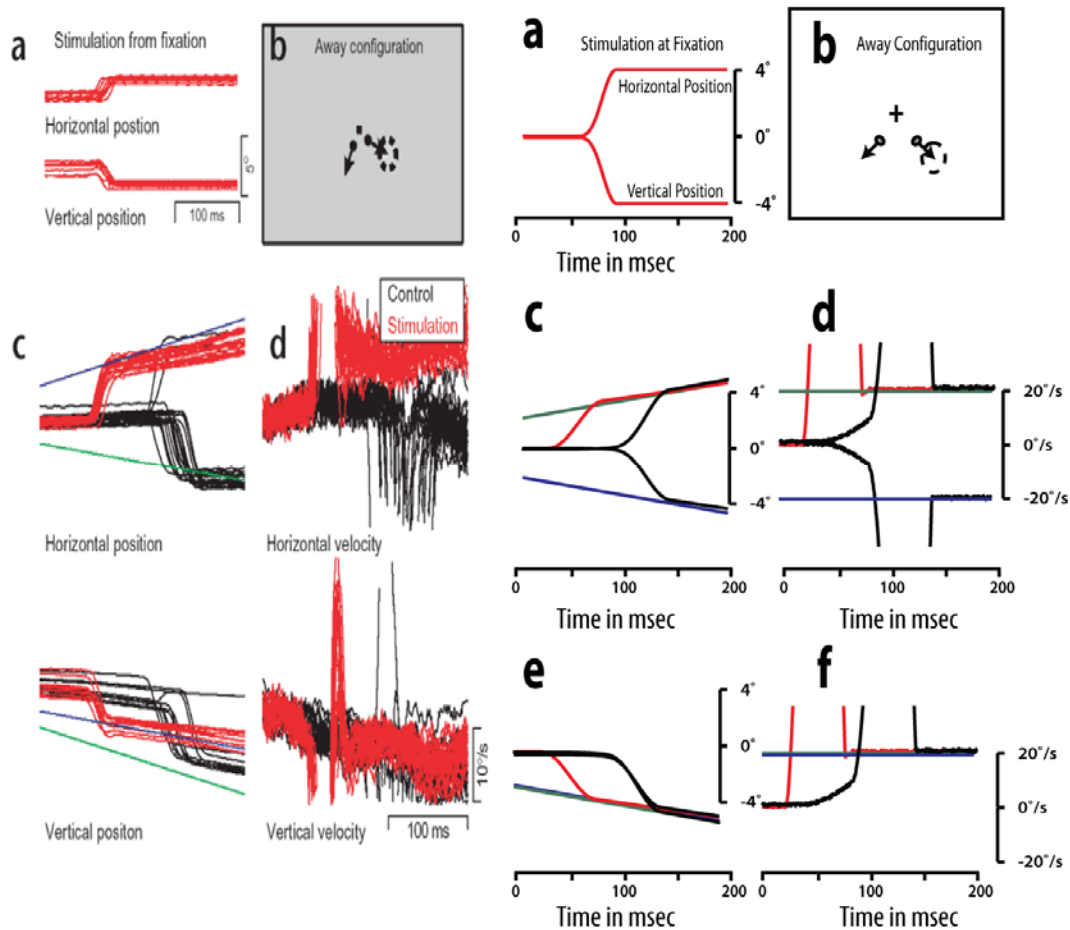


Figure 10: Saccadic choice drives smooth pursuit choice. The Figure illustrates how saccadic choice, when forced via FEF stimulation, drives a corresponding choice within the SPEM system. Panel (a) shows vertical and horizontal eye position traces when the FEF was stimulated at a sampled location during fixation in phase one of the experimental paradigm (Gardner and Lisberger, 2002) simulated. In this case, stimulation evoked a 4 deg oblique saccade and allowed the experimenters to predict the part of the visual field from

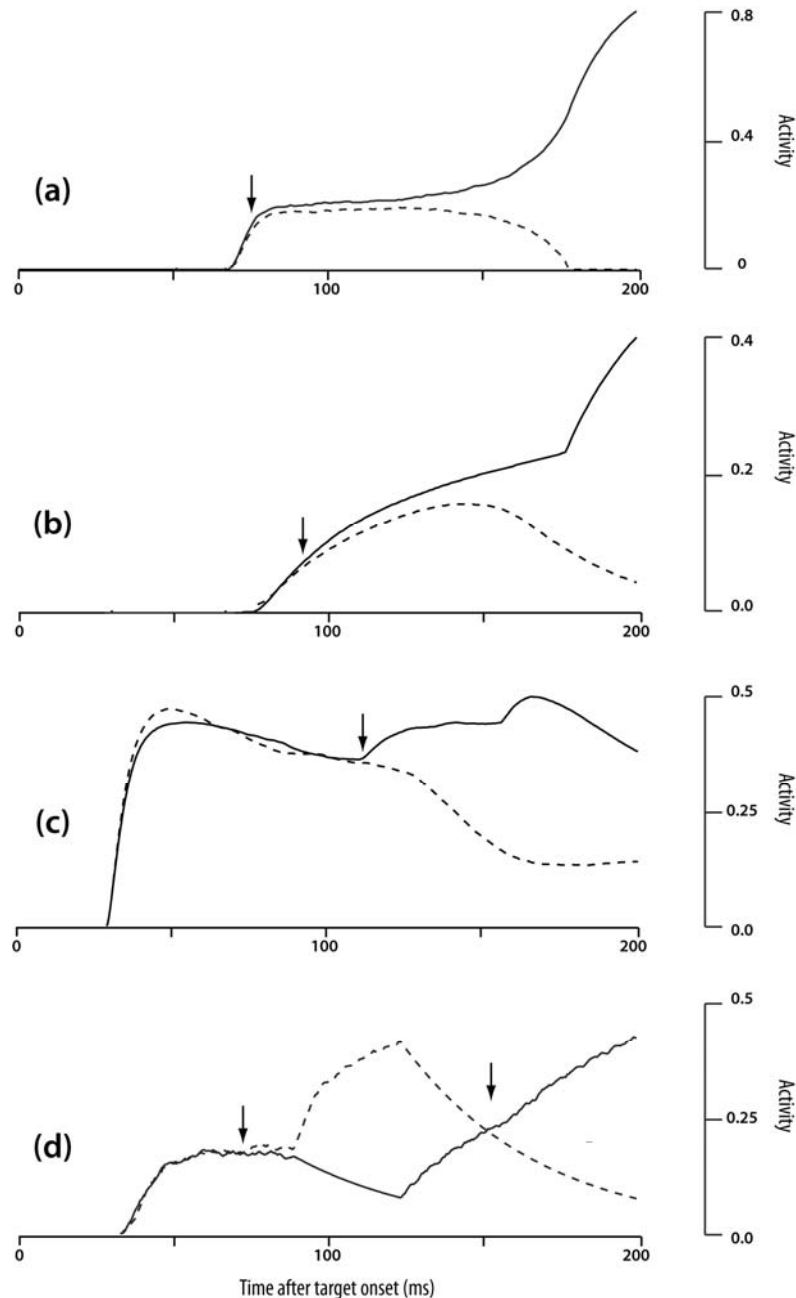
which the same cell could be activated. Panel (b) illustrates that in phase two, they then made two stimuli appear at the same eccentricity on two sides of the fixation point. They start moving away from each other, such that one of the stimuli would enter the previously mapped FEF cell's movement field. If that FEF cell is stimulated just as the target enters its movement field and before a natural saccade is initiated, then the SPEM system will always choose to pursue that target rather than the alternative. Panels (c) and (d) show horizontal position and velocity traces respectively. Similarly, panels (e) and (f) show vertical position and velocity traces. Blue and green lines show the traces of kinematic variables for the two moving stimuli. Black traces show the relatively long-latency, natural catch-up saccades to either stimuli on trials with no FEF stimulation, whereas red traces show the relatively short-latency saccades evoked by FEF stimulation. Eye velocity after the saccade matches exactly that of the target near its current position, whether the target was naturally chosen or chosen by FEF stimulation.

Figure 11 shows the predicted activation dynamics for two competing cells at each of five stages of the model during an episode in which a SAC choice overrides a SPEM choice. The series of panels, from top to bottom, corresponds to the path of information transfer, across involved stages, for communicating the choice from the SAC to the SPEM system. Thus, Figure 11a plots FEF planning neurons; Figure 11b, LIP saccadic neurons; Figure 11c, MST_v direction cells; and Figure 11d, FPA output averaging cells. Solid lines represent the traces of cells whose preferred directions match the stimulus that is eventually chosen as target by the SAC system. In Figure 11d, the FPA stage of the SPEM system initially chooses the other stimulus (dashed trace; see first arrow in Figure 11d). Note that the time at which FPA flips its choice (second arrow in Figure 11d) is mere milliseconds after FEF makes its choice. This allows the SPEM system to establish a good representation of the new target's velocity before the saccade is actually generated. This enables the post-saccadic SPEM to exhibit a velocity that is already matched to the target velocity.

Discussion

Primates use a combination of saccadic and smooth pursuit eye movements to track a selectively attended moving object. Recent data, on monkeys performing a target selection task, indicate that each system has its own selection mechanism, but that in the event of a conflict, the SAC system's choice overrides the choice made by the SPEM system (Adler et al., 2002; Ferrera and Lisberger, 1995; Gardner and Lisberger, 2001, 2002; Horwitz and Newsome, 2001). This paper and its companion (Grossberg et al., 2007) describe a neural circuit model that is capable of simulating these and a large number of additional data concerning how the SAC and SPEM systems interact to select and track targets among distractors in a coordinated way.

In our model, saccadic target selection emerges from interactions of frontal, parietal and collicular regions with the basal ganglia. Visually responsive cells in FEF, SC and LIP show target/distractor discrimination at about the same time after target onset: FEF, 130-150 ms (Schall, Hanes et al., 1995; Thompson et al., 1996); SC, 110 – 130 ms (McPeck & Keller, 2002); LIP, 132 ± 2.3 ms (Thomas & Pare, 2007). However, when compared with respect to saccadic initiation time, $t = 0$, larger population of FEF and SC cells show earlier activity FEF, 78% at $t = -53$ ms; SC, 98% at $t = -45$ ms; LIP, 60% at $t = -26$ ms. This accords with our claim that FEF and SC plan and execute a saccade and this information is passed to LIP to coordinate and plan further eye movements.



*Figure 11: Simulating how target selection by the SAC system overrides prior choice by the SPEM system. The Figure shows model simulations of the paradigm used by Krauzlis and by Adler et al. If SPEM tracks one of two moving stimuli before a saccade to the other, the pos-saccadic SPEM always has a velocity appropriate to the saccadic target. Simulated activities of FEF planning (panel **(a)**), LIP saccadic (panel **(b)**), MST_v (panel **(c)**) and FPA (panel **(d)**) output (“averaging”) neurons are shown. The thick black line in each denotes the activity of a neuron containing the final target for SAC and SPEM within its RF. The dotted line represents the activity of a neuron containing the stimulus that attracted the initial SPEM within its RF. All activities are synchronized with target onset time. Arrows in each panel indicate the time when the first (and, if present, the second) sign of selectivity is observed. In panel **(d)**, the first arrow indicates the SPEM system’s initial target selection.*

The second arrow indicates SAC choice overriding the SPEM system's earlier selection. The SAC choice is conveyed from FEF to FPA via the LIP-MT-MST-FPA pathway (Figure 6). The time line of arrows illustrates this transfer. The SAC choice bias starts to grow at 75ms. This evolving bias is conveyed to LIP and becomes visible around 90 ms, and appears in MSTv at 110 ms. It takes another 40 ms for FPA to flip its choice.

The anatomical loci and processes that are most critical for SPEM target selection are still unsettled. Our model is based on the hypothesis of a partial parallelism between the SAC system and the SPEM system. Notably, SPEM target selection emerges as a result of interactions between the basal ganglia and a frontal area, the FPA. Stimulation of the FPA, or any other region downstream from it in the SPEM circuit, notably NRTP or a pursuit zone of the cerebellum, causes SPEM within a very short latency: FPA, 25-35 ms (Gottlieb et al., 1993; Tanaka and Lisberger, 2002b); NRTP, 20 ms (Yamada et al., 1996); CBM, 10 ms (Belknap & Noda, 1987). This is also true in the model. However, stimulating upstream from FEF, at MST or MT, modulates existing pursuit but never evokes SPEM from a voluntarily maintained fixation (Komatsu & Wurtz, 1989). The same would be true in the model if it were augmented to include a STOP-signal channel to complement the GO-signal channel. Such a STOP-signal channel could suppress voluntary fixation responses to MT and MST stimulation in a manner analogous to that shown for the SAC system in Brown et al. (2004). These considerations reinforce the hypothesis of partial SAC-SPEM parallelism, and the more specific hypothesis that the voluntary gating associated with SPEM target selection occurs in FPA, which connects with the BG-Thalamus system in a way that is analogous to FEF.

Before noting the limits of the parallelism in our model, it is useful to consider and evaluate an alternative view. There is growing evidence for rostral SC (rSC) involvement in pursuit. Some non-fixation neurons in rostral SC show target/distractor discrimination. Stimulation of rostral SC inhibited pursuit in the ipsilateral visual hemifield but had little effect on ongoing pursuit of targets in the contra-lateral hemifield (Basso, Krauzlis, & Wurtz, 2000; Krauzlis, Basso, & Wurtz, 1997; Krauzlis et al., 2000). Stimulation also increased the probability of selecting a stimulus that appeared contra-lateral to the site of stimulation irrespective of target motion direction (Carello & Krauzlis, 2004). rSC thus shows two necessary properties for target selection: target/distractor discrimination and forced bias via stimulation. However, stimulation of rSC does not generate SPEM, and the bias generated by the rSC stimulation is irrespective of the direction of target motion. One possible explanation for these two effects comes from the bilateral connections between SC and LIP. LIP sends collaterals to the intermediate and deep layers of SC (Lynch, Graybiel, & Lobeck, 1985) and gets return projections from SC via pulvinar (Clower, West, Lynch, & Strick, 2001). LIP shows both these properties for SAC target selection and so, rSC activity might simply reflect the activity of foveal LIP cells during SPEM.

Although the model's SPEM and SAC sub-systems each use a frontal-BG-Thalamic loop for voluntary gating of target selection, there are some notable differences in the connectivity in the current version of the model. In the SAC system, FEF planning cells, SC buildup cells, and LIP cells all project to the BG-Thalamus decision stage and help choose the target. Grossberg et al. (1997) modeled how activity representing multiple possible saccadic targets can coexist during the preparatory phase in the deeper layers of SC, until competition determines the final choice of saccadic target. Gancarz and Grossberg (1999) further developed these ideas to predict

and simulate how FEF and SC may work together to determine a saccadic choice. The current model further develops these concepts.

In particular, the FEF motor output cells are distinct from the planning cells, and do not become active enough to drive downstream SAC generators until they receive a GO signal from the BG-Thalamus decision stage. In contrast, FPA averaging cells, which are here modeled as the FPA cells that send outputs to downstream SPEM generators, are the sole source of input to the SPEM part of the BG-Thalamus decision stage, as well as the sole cortical recipient of the GO signal that initiates high-gain pursuit. Given a low threshold for SPEM initiation downstream from the FPA, the current model cannot avoid exhibiting a phase of low-gain vector-averaging SPEM before the BG-Thalamus decision process forces a choice and initiates high-gain pursuit of whichever target direction representation survives the enhanced competition induced by the action of the GO signal.

This lack of full parallelism between the FEF-BG-Thalamus and the FPA-BG-Thalamus circuits is in accord with data indicating that vector averaging is much more common in the SPEM than in the SAC system. This may be because the visual consequences of SAC vector averaging are highly negative. The same is not true for SPEM vector averaging. In any case, some other variants of the SPEM circuit are also compatible with the data and computational constraints (Figure 6). For example, similar behavior can be achieved if both the MST_v -recipient WTA and averaging cells of the FPA project to the BG-Thalamus decision stage, provided that weights and thresholds are adjusted accordingly. What would not work would be a projection from the model FPA's MST_d -recipient summation cells to the BG, if they have a large relative weighting. Such a circuit would exhibit mid-pursuit failures of the GO signal, because the discharge rate of the summation cells declines sharply during maintained successful pursuit. This is because the MT cells that drive them lose their major excitatory input when successful pursuit cancels target motion in the retinal frame. In contrast, the MST_v cells (which ultimately drive FPA WTA and averaging cells in the current model) receive an efference copy signal that sustains their discharge during successful pursuit (Pack et al., 2001).

What pathway ensures coordination between the SAC and SPEM systems if their decisions are initially in conflict? The model embodies the hypothesis that LIP possesses characteristics suitable for acting as a conduit for a multi-step transfer of information between the SAC and SPEM systems. Alternatively, it might be proposed that SAC target choice could be transferred to the SPEM system in a single step, via a direct projection from FEF to FPA. Although these regions are nearby, no such direct projection is known. How such a projection might be made to work is also unclear because of incongruent representations at FEF and FPA. FEF has a retino-centric vector map, such that each cell explicitly codes a saccade having a particular magnitude and direction and implicitly codes a single retinotopic locus. FPA, on the other hand, has a directional map, such that each cell explicitly codes a preferred direction of SPEM motion regardless of the target's retinotopic locus. So any direct "alignment" could only be based on directions, not on retinotopic positions. As such, any would-be selective signal from FEF to FPA would be ambiguous: There might be many targets moving in the same direction, but at different positions on the retina.

To effect the transfer of choice from SAC to SPEM, the model instead incorporates the well-established projection from FEF to LIP to MT. The transfer can be unambiguous as to retinal locus because FEF, LIP and SC all embody *retino-centric* maps. In the model, each region is represented by a 15x15 grid with the center [7, 7] representing the fovea. The LIP to MT projection can be thought of as a position-based attentional bias signal. This assumption is in

tune with data that show MT/MST neurons increasing their activity if a target is present within their retinotopic receptive fields. Enhancement ranges from ~9%, for random dot coherent motion stimuli (Seidemann & Newsome, 1999), to ~25 - 35% for single-stimulus motions (Ferrera and Lisberger, 1997; Treue and Maunsell, 1999). In accord with this, model MT cells whose receptive fields overlap the retinotopic position of the SAC target choice get a boost in input. This accords with data that spatial cues reduce latency of eye movement generation more than form or motion cues (Adler et al., 2002). Of course, spatial cueing by itself is sometimes insufficient. Because the model has no feature or form representations, in its current form it cannot simulate how the real SAC system could force a choice, based on color or form, between two moving stimuli falling within the same LIP receptive field.

Once the same stimulus is selected as a target, the SAC and SPEM systems must make further decisions and adjustments to produce the kind of tracking that optimizes visual and cognitive processing of the object. Even in the rare case of linear, constant-speed object motion, target speed can easily exceed the maximum SPEM speed, so further decisions include when to generate catch-up saccades. Because catch-up saccades may overshoot, and because jump-back saccades degrade vision, further intelligent adjustments include briefly lowering pursuit gain (the ratio of SPEM velocity to target velocity) below unity, in order to allow the target to more quickly catch-up with the moving line of gaze. A companion paper about the model (Grossberg et al., 2007) treats a large number of such coordination examples, and shows a good match between simulation results and experimental data.

Supplementary Material

The model is designed to capture key aspects of the processing of visual and motor signals in saccadic and smooth pursuit areas. The model simulates cell responses in such areas (Figure 1) through the use of nonlinear differential equations based on the classical membrane equation (Grossberg, 1973, 1982; Hodgkin, 1964). The system of equations was numerically integrated using the fourth order Runge-Kutta method, with a fixed step size of 0.001.

Visual Inputs. Each visual input to the smooth pursuit circuit is a vector field that describes the speed of the motion at each point (x, y) . The values of x and y are each constrained to be between $[-1, 1]$ which is mapped to $[-60^\circ, 60^\circ]$ in visual space. The velocities $v(x, y)$ are constrained between the values $[0, 1]$. The target is a square block of length and width r moving in any one of the eight cardinal directions in the visual field. The center of the object is given by (x_0, y_0) and its speed is v_0 . The retinal image velocity, $v'(x, y)$, is calculated as the difference between object speed and the eye speed at that point. Target visibility is controlled by two variables T_{on} and T_{off} , which specify the on and off times of the target in the simulation. Fixation offset is marked by T_{fix} set equal to 500.

MT Cell. The cells representing the input for the smooth pursuit circuit are modeled after cells found in the middle temporal area (MT). MT cells have speed and direction tuning (Maunsell & Van Essen, 1983). Two different types of cells have been observed in MT. One type, MT^- cells, respond vigorously to small stimuli moving in their receptive field at a particular speed and in a particular direction. The second type, MT^+ cells, respond to large stimulus sizes. There is a large MT projection to MST. MST also has two major cell types. Cells in ventral MST (MST_V) show direction-sensitive modulation to object motion (Tanaka, Sugita, Moriya, & Saito, 1993). Cells found in dorsal MST (MST_D) respond to large field stimulus motion. These target tracking and navigation cells are computed using complementary subtractive vs additive operations (Grossberg, 2000; Grossberg, Mingolla, & Pack, 1999; Pack, Grossberg, & Mingolla, 2001).

We simulated 100 model MT cells for each of the eight cardinal directions (800 cells total). Each cell had a preferred speed and direction. The receptive field (i, j) was constrained to be between $[-1, 1]$. The speed tuning of a cell at position (i, j) is defined by a Gaussian function, G_{ijxy}^v , centered on a preferred speed v_{ij} . The direction tuning was also a Gaussian function, G_{ij}^d , centered on the preferred direction d_{ij} .

Each MT cell has a receptive field size dictated by the eccentricity of the cell from the fovea. Cells that are farther from the fovea have bigger receptive fields in keeping with the cortical magnification factor. The width of each receptive field, W_{ij} , as a function of the cell's position in retinotopic space, is given by

$$W_{ij} = \frac{25}{0.91(i^2 + j^2)^{0.5} + 1.0}. \quad (1)$$

Each MT cell has a preferred direction which is selected at random from any of the eight cardinal directions. It also has a preferred velocity, v_{ij} , chosen from the distribution $e^{-Q(v-0.5)^2}$. Only inputs matching these directional preferences activate the cell. For each MT cell, the total response to a motion stimulus was characterized in terms of center-surround inputs to that MT cell. The on-center response, α_{ij}^+ , of the receptive field to a visual target depends on the presence of three factors: the position (x, y) of the target within its receptive field, the velocity $(v(x,y))$ of the target near the preferred velocity (v_{ij}) , and the direction (d) of the target along or near the preferred direction (d_{ij}) of the cell, namely:

$$\alpha_{ij}^+(v_{ij}, d_{ij}) = \sum_{x,y} G_{ijxy}^{cp} G_{ijxy}^v G_{ij}^d. \quad (2)$$

In (2), G_{ijxy}^{cp} represents the position sensitivity of the cell. It decreases as the target moves away from the center of the MT response field by:

$$G_{ijxy}^{cp} = e^{-W_j[(i-x)^2+(j-y)^2]}. \quad (3)$$

Similar to position sensitivity, G_{ijxy}^v represents the velocity tuning of the MT cell. This term reaches its maximal value if the velocity of the target ($v(x,y)$) is the same as the preferred velocity (v_{ij}) of the cell:

$$G_{ijxy}^v = e^{-G_1(v_{ij}-v(x,y))^2}. \quad (4)$$

MT cell activity also depends on the direction (d) of target motion relative to the cells preferred direction (d_{ij}). This term can be calculated as:

$$G_{ij}^d = e^{-G_2(d_{ij}-d)^2}. \quad (5)$$

Parameters G_1 and G_2 , in equations (4) and (5) equal 10 and 6, respectively.

MT cells also receive input from surround regions α_{ij}^- , chosen to be five times the size of the on-centers:

$$\alpha_{ij}^-(v_{ij}, d_{ij}) = \sum_{x,y} G_{ijxy}^{sp} G_{ijxy}^v G_{ij}^d. \quad (6)$$

In (6), the position sensitivity (G_{ijxy}^{sp}) is calculated as

$$G_{ijxy}^{sp} = e^{-\frac{W_j[(i-x)^2+(j-y)^2]}{25}}, \quad (7)$$

and G_{ijxy}^v and G_{ij}^d are defined as in equations (4) and (5).

The model computes MT^+ cell activities by *adding* the surround to the center component, and MT^- cells by *subtracting* the surround from the center component.

Subtractive Cells (MT^-). A model MT^- cell input is given by:

$$\beta_{ij}^-(v_{ij}, d_{ij}) = [\alpha_{ij}^+(v_{ij}, d_{ij}) - \alpha_{ij}^-(v_{ij}, d_{ij})]^+, \quad (8)$$

and its activation dynamics are described by:

$$\frac{dm_{ijvd}^-}{dt} = -m_{ijvd}^- + (1 - m_{ijvd}^-)(\beta_{ij}^-(v_{ij}, d_{ij}))(1 + [s_d^-]^+) + \sum_{ab} a_{ab} W_{abij} - (1 + m_{ijvd}^-) \sum_{e \neq d} s_e^-. \quad (9)$$

Apart from the directional tuned input ($\beta_{ij}^-(v_{ij}, d_{ij})$), model MT^- also receives top-down modulatory excitatory input from the MST_V cell (term $[s_d^-]^+$) having the same directional preference as the MT^- cell and from LIP (term $\sum_{ab} a_{ab} W_{abij}$). It is also inhibited by MST_V cells tuned to different directions (term $\sum_{e \neq d} s_e^-$) as part of the top-down attentional MST_V feedback.

Term $\sum_{ab} a_{ab} W_{abij}$ in equation (9) and (12) represents an excitatory input from an LIP neuron with a retinotopic receptive field (W_{abij}) that is in register with that of the recipient MT neuron:

$$W_{abij} = \begin{cases} 1 & \text{if } a - \delta/2 < i < a + \delta/2 \text{ and } b - \delta/2 < j < b + \delta/2 \\ 0 & \text{otherwise} \end{cases} \quad (10)$$

In (10), δ represents the diameter of LIP neurons response field. Thus, $\sum_{ab} a_{ab} W_{abij}$ enables a saccadic decision to enhance MT and MST processing of a selected target.

Additive Cells (MT⁺). A model MT⁺ cell's net center-surround input is given by:

$$\beta_{ij}^+(v_{ij}, d_{ij}) = \alpha_{ij}^+(v_{ij}, d_{ij}) + \alpha_{ij}^-(v_{ij}, d_{ij}), \quad (11)$$

and its activation dynamics are described by

$$\frac{dm_{ijvd}^+}{dt} = -m_{ijvd}^+ + (1 - m_{ijvd}^+) (\beta_{ij}^+(v_{ij}, d_{ij}) (1 + [s_d^+]^+) + \sum_{ab} a_{ab} W_{abij}) - (1 + m_{ijvd}^+) \sum_{e \neq d} s_e^+. \quad (12)$$

MT⁺ cells also receive excitatory input from MST cells, but from the dorsal sub-region (term s_d^+) as compared to the ventral sub-region for MT⁻ cells. They also receive an excitatory input from LIP (term $\sum_{ab} a_{ab} W_{abij}$), as well as inhibition ($-\sum_{e \neq d} s_e^+$), from MT⁻ recipient MST_D cells coding for non-matching directions.

The top-down inputs from MST to MT are consistent with data (Seidemann & Newsome, 1999; Treue & Maunsell, 1999) indicating that MT cell activity is modulated by top-down attention. This top-down modulatory on-center, off-surround circuit has been shown capable of focusing attention while also stabilizing learning in the network (Carpenter & Grossberg, 1993; Grossberg, 1980; Grossberg, 2003).

MST Cells. Inputs from model MT cells with varying speed selectivities but similar directional preferences are pooled by direction-tuned, speed-sensitive cells in the model MST. MT⁻ cells project to MST_V and MT⁺ cells project to MST_D. The MST_D activities are symbolized by s_d^+ , and the MST_V activities by s_d^- , where subscript d indicates the cell's direction preference and D indicates direction anti-parallel to cell's preferred direction. Direction “ d ” takes the values 0°, 45°, 90°, 135°, 180°, 225°, 270°, 315°.

Target tracking Cells (MST_V). Target tracking cells in MST (s_d^-) calculate an estimate of predicted target velocity during pursuit. Their input comes from retinal sources (from MT) and extra-retinal sources (via a corollary discharge) and thus can provide a reliable estimate of target velocity even during sustained pursuit. The activities of the small-field MST_V cells are given by:

$$\frac{ds_d^-}{dt} = -s_d^- + (1 - s_d^-) [2.5 \sum_{ij} [m_{ijvd}^-]^+ v_{ij} + 5.5 [s_D^+]^+ + 2(k_d - k_D)]^+ - 75 \sum_{e \neq d} s_e^-. \quad (13)$$

In (13), term $\sum_{ij} m_{ijvd}^- v_{ij}$ gives an estimate of the average velocity computed by the MT⁻ cells having the same direction preference. Other sources of excitatory input come from the large-field MST_D cell having an opposite direction to this MST_V cell (term s_D^+), and via corollary discharge ($k_d - k_D$) (see Pack et. al. (2001)). There is also mutual inhibition between the MST_V cells coding other directions (term $-75 \sum_{e \neq d} s_e^-$).

Input from MST_D cell having an opposite direction to MST_V cell that represents a pursued target to be excited by the background counter-motion generated by SPEM. Such excitation helps MST_V to better compute predicted target velocity when visual motion inputs

decrease from MT^- cells to MST_V cells during successful pursuit. In equation (13), k_d is a corollary discharge, or efference copy, from the pursuit neurons of the vestibular nucleus that fire when the eye moves in direction d (see equation (26) below), and k_D is the corollary discharge from pursuit neurons that fire when the eye moves in the direction D that is opposite to d . Term k_d is calculated as a mix of the two nearest orthogonal signals θ and $\theta + 90^\circ$ to d from the values $0^\circ, 90^\circ, 180^\circ$ and 270° :

$$k_d = \sqrt{h_\theta^2 + h_{\theta+90}^2}. \quad (14)$$

These corollary discharge signals, which grow as the eye velocity grows to match the velocity of the SPEM target, can also compensate for the reduction of small-field visual motion signals that attend any successful SPEM. The result is that MST_V cells can provide a reliable estimate of predicted target velocity throughout a SPEM episode, namely before SPEM onset, during SPEM acceleration, and during steady-state matching of eye to target velocity.

Motion opponency of the efference signals ($k_d - k_D$) in equation (14) supports this type of activity profile. During SPEM onset, $[k_d - k_D]$ is zero. Once the eye starts to move, $[k_d - k_D]$ becomes excitatory for MST_V cells aligned along direction of target motion and inhibitory for the MST_V cells in the opposite direction. This pattern is reversed for MST_D cells as seen in the equation (15).

Navigation Cells (MST_D). MST_D cell get input from the large receptive field MT^+ cells having same directional preference, and so is sensitive to coherent background motion. The activities of the large-field MST_D cells are given by:

$$\frac{ds_d^+}{dt} = -s_d^+ + (1 - s_d^+) [0.1 \sum_{ij} [m_{ijvd}^+] + 5.5 [s_d^-] + 2(k_D - k_d)] - 15 \sum_{e \neq d} s_e^+. \quad (15)$$

The excitatory input to MST_D cells comes from three sources: MT^+ cells ($\sum_{ij} m_{ijvd}^+$) having the same directional preference as the model MST_D cell, the MST_V cell (s_d^-) having the same directional preference, and via corollary discharge ($k_D - k_d$). There is mutual inhibition between the MST_D cells coding other directions (term $-15 \sum_{e \neq d} s_e^+$). Note that the corollary discharge input ($k_D - k_d$) to the cell is the opposite of the corollary discharge to MST_V cell (see equation (13)). This opponency ensures that, during sustained pursuit, the activity of MST_D cells tuned to background motion direction remains bounded and does not affect the current pursuit dynamics.

FPA Cells: The frontal pursuit area (FPA) is considered to be the first area where a sensory-to-motor transformation of SPEM signals takes place. The model FPA contains three cell types that model cells reported in literature (Tanaka & Lisberger, 2002a):

Winner-Take-All cells (WTA). WTA cells receive input from target-tracking cells of MST and convey this information to the target-selective FPA vector averaging cells. Their activity, f_d^I , obeys:

$$\frac{df_d^I}{dt} = -2f_d^I + (1 - f_d^I)(50[s_d^-] + 10f_d^R) - 10 \sum_{e \neq d} f_e^I. \quad (16)$$

By (16), these cells are excited by MST_V cells (term $50[s_d^-]$) having the same directional preference, and by self excitatory interneurons (term $10f_d^R$). There is mutual inhibition among

input cells with different direction preferences (term $-10\sum_{e \neq d} f_e^I$). The excitatory interneurons within the input layer support self-sustaining activity:

$$\frac{df_d^R}{dt} = -f_d^R + (1 - f_d^R)[f_d^I]^+. \quad (17)$$

Vector Summation cells. Vector summation cells receive input from the navigation cells of MST and provide additional acceleration during pursuit initiation. These activities obey:

$$\frac{df_d^S}{dt} = -f_d^S + (1 - f_d^S)15[s_d^+]^+ - (1 + f_d^S)\sum_{e \neq d} f_e^S. \quad (18)$$

Summation cell activities (f_d^S) are excited by MST_D cells of the corresponding direction (term $15s_d^+$), and have low mutual inhibition (term $-\sum_{e \neq d} f_e^S$). This inhibition enables two stimulus directions to be simultaneously active and enables vector averaging to occur before target selection.

Vector Averaging Output cells. Model vector averaging cells perform the role of target selection cells in the SPEM system. These cells interact with basal ganglia via thalamus and help decide the target stimulus among many distractors. These activities obey:

$$\frac{df_d^O}{dt} = -10f_d^O + (1 - f_d^O)(15[f_d^I]^+ + [f_d^S]^+ + 15\mu^d + 1.5[g^P - 0.5]^+) - 25(1 + f_d^O)\sum_{e \neq d} f_e^O. \quad (19)$$

FPA output activities (f_d^O) are excited by FPA input cells (term $15f_d^I$) and summation cells (f_d^S) having the same direction preference, by electrical stimulation (μ^d), and by a cortico-thalamic decision signal ($[g^P - 0.5]^+$). The cortico-thalamic decision signal helps in target selection when more than one stimulus is present in the environment. The output cells receive strong inhibitory input from output cells with different direction preferences (term $-25\sum_{e \neq d} f_e^O$). If

several FPA input cells are active at the same time, indicating more than one moving target, the output cells show a reduced response due to this inhibitory process.

Model FPA output cells carry the estimate of target velocity. FPA WTA cells (see equation (16)) receive direct inputs from MST_V cells which estimate the target velocity. This activity is sustained even during target blink via the self-excitatory interneuron. During single stimulus tracking, FPA output cells carry the target velocity estimate from MST_V to NRTP. When multiple stimuli are present, FPA input cells hold the representations of all stimuli until FPA output cells decide the target among the distractors. Once FPA output cells select a target for a future SPEM, the activity of FPA input cells representing the distractor starts decaying.

Decision signal (g^P). Onset of the gating signal g^P in (19) occurs once the total activity reaches 0.5. Then, BG-Thal sends a nonspecific signal that boosts the activity of all the FPA averaging cells. Mutual inhibition helps choose the winner. Thus, this interaction results in a choice that is controlled by a cortico-basal ganglia-thalamocortical loop (Basso & Wurtz, 2002; Brown et al., 2004). Its value is calculated as:

$$\frac{dg^P}{dt} = -0.2g^P + (1 - g^P)\sum_d [f_d^O - 0.33]^+. \quad (20)$$

In (20), g^P is activated by a thresholded input from FPA output cells (f_d^O). When g^P exceeds 0.5 (see equation (19)), the FPA output cell with maximal activity is chosen as the target and the competition is silenced via strong mutual inhibition.

Pontine nuclei. Pontine nuclei act as way stations for the SPEM information transfer from cortex to cerebellum. We have modeled two important pontine nuclei, namely DLPN and NRTP.

DLPN Cells. DLPN cells have large receptive fields covering almost the whole contra-lateral visual field and have directional preferences and speed selectivities similar to MT cells. There is no topographic arrangement of cells in DLPN. The activities of DLPN cells obey:

$$\frac{dp_{vd}^D}{dt} = -p_{vd}^D + 0.1(1 - p_{vd}^D) \sum_{ij} [m_{ijvd}^-]^+ - 100(1 - p_{vd}^D) \sum_{\substack{e \neq d \\ f \neq v}} p_{fe}^D. \quad (21)$$

By (21), DLPN cells receive convergent excitatory inputs from all MT^- cells of the same speed and direction (term m_{ijvd}^-). Mutual inhibition among DLPN cells (term $-100 \sum_{\substack{e \neq d \\ f \neq v}} p_{fe}^D$) enables

only those neurons whose velocity tuning is close to that of the target velocity to remain active. Therefore, model DLPN cells output an approximate estimate of target velocity without regard to its specific retinotopic locus. This approximate estimate provides drive to the initial eye acceleration (see equation (24)) and helps the cerebellum make corrections to the amplitudes of saccades made to moving targets (see equation (70)).

NRTP Cells. Two types of pursuit-related cells have been observed in NRTP: acceleration cells and velocity cells (see Simulation 2 and Figure 4). We predict that the acceleration cells act within an internal negative feedback loop to compute the difference between estimated target velocity and eye velocity. The velocity cells integrate acceleration cell output.

NRTP Acceleration cells: NRTP acceleration cell output acts as a mismatch detector between the estimates of target and eye velocities. The activities of these cells obey the equation:

$$\frac{dp_{ad}^N}{dt} = -p_{ad}^N + 45(1 - p_{ad}^N) [f_d^O - k_d]^+ - 50 \sum_{e \neq d} p_{ae}^N. \quad (22)$$

The acceleration cells (p_{ad}^N) are excited by the difference between f_d^O , the FPA output that estimates target velocity, and k_d , the vestibular nuclei (rLVN/ MVN, see equation (14)) output that controls, and thus estimates, eye velocity. There is also mutual inhibition between different NRTP acceleration cells ($-50 \sum_{e \neq d} p_{ae}^N$).

NRTP Velocity cells: The activities of these cells follow the equation:

$$\frac{dp_{vd}^N}{dt} = -0.4 p_{vd}^N + 40(1 - p_{vd}^N) [p_{ad}^N]^+. \quad (23)$$

Acceleration cell activity p_{ad}^N in equation (22) is the only excitatory input to the velocity integrator cells.

CBM Cells. The model cerebellum is highly simplified. It channels sub-cortical SPEM information from NRTP and DLPN towards the vestibular nuclei which control the eye muscles. Hence, cerebellectomy results in large and lasting deficits in pursuit (Zee, Yamazaki, Butler, & Gucer, 1981). The activities of these cells are given by:

$$\frac{dc_d^P}{dt} = -0.5c_d^P + (1 - c_d^P)(10 \sum_v [p_{vd}^D]^+ + 20p_{vd}^N) - 25(1 + c_d^P) \sum_{e \neq d} c_e^P. \quad (24)$$

The cerebellum cell activities c_d^P are directionally tuned and receive excitatory input from DLPN ($\sum_v p_{vd}^D$) and NRTP (p_{vd}^N) from both hemispheres. Mutual inhibition occurs across directions ($-25 \sum_{e \neq d} c_e^P$). Since cerebellum cells are velocity sensitive but not velocity tuned, the DLPN cell input is pooled over all velocities along a particular direction.

rLVN/MVN cells. Vestibular nuclei (medial and rostro-lateral vestibular nuclei) represent the penultimate stage of processing for SPEM. Here the directional representation is broken down from its cardinal axes into axes along which the muscle can move the eye. Since there are eight cardinal directions (d) represented by the model cerebellar pursuit cells and there are 4 orthogonal directions in which the muscle can move the model eye (represented by θ), the outputs from three cerebellum cells form one rLVN/MVN input. For example, the rLVN/MVN input along the upward direction ($\theta = 90^\circ$), is defined by adding the cerebellar cells that are active for top-right ($d = 45^\circ$), top ($d = 90^\circ$), and top-left ($d = -45^\circ$) directions:

$$I_\theta^P = c_{\theta-45^\circ}^P + c_\theta^P + c_{\theta+45^\circ}^P. \quad (25)$$

Pursuit neuron activities in the rLVN/MVN are defined by:

$$\frac{dh_\theta}{dt} = -0.6h_\theta + 4I_\theta^P - 1.5I_\Theta^P - 7.5v(o). \quad (26)$$

By (26), these cells receive pursuit input ($4I_\theta^P$) from the cerebellum. They are inhibited by opponent direction pursuit input ($-1.5I_\Theta^P$) and by the omnipause neurons ($-v(o)$) in the brain stem. The signal function $v(x)$ is a sigmoid, calibrated such that inhibition from OPNs during pursuit is not enough to totally inhibit activity of pursuit neurons. It is given by:

$$v(x) = \frac{x^4}{x^4 + 0.5^4}. \quad (27)$$

During sustained pursuit, the inhibition from OPNs is high, but not strong enough to inhibit pursuit activity. During saccades, OPNs become silent and this causes the inhibition to become zero and helps pursuit neurons to reach the target velocity faster (post-saccadic enhancement of eye velocity, see Simulation 2). As above, direction θ takes the values of 0° , 90° , 180° and 270° , which represent rightward, upward, leftward and downward directions of motion. Parameter Θ in equation (26) is defined as: $\Theta = \theta + 180^\circ$.

OPN cells. Omnipause neurons (OPNs) are tonically active cells present in the nucleus raphe interpositus and are known to inhibit saccades. They are active during periods of sustained pursuit and fixation, but become silent during saccades. The model OPN activities follow Gancarz and Grossberg (1999) and are defined as:

$$\frac{do}{dt} = -0.2o + (1 - o)(1.2 + 20[u_{ff}]^+) - 3.5(o + 0.4)(20v(l_\theta) + 5v(h_\theta)). \quad (28)$$

Model OPNs are excited by a constant arousal signal (term 1.2) and SC fixation cell output (term u_{ff} , see equation (42)). These two sources of OPN activation are consistent with neurophysiological data showing that OPNs can discharge even when fixation neurons are silent (Everling et al., 1998).. These cells are inhibited by long lead burst neurons ($v(l_\theta)$), see equation

(73)) as well as pursuit neurons ($v(h_\theta)$, see equation (26)), but by varying degrees. The sigmoidal signal function ($v(x)$) obeys:

$$v(x) = \frac{x^4}{x^4 + 0.1^4}. \quad (29)$$

The strength of inhibition from long lead burst neurons is stronger than pursuit neurons because OPNs go silent during saccades but are active at 66% of their maximal value during maintained pursuit (Missal & Keller, 2002).

SC Cells. The model SC includes two cell layers or maps: SC burst cells and buildup cells (Munoz & Wurtz, 1993a, 1993b, 1995a, 1995b). SC receives collaterals from FEF, LIP and from LGN. Activities of these cells are represented by equations which are similar to equations in Gancarz and Grossberg (1999).

SC Burst Cells. Model SC burst cells represent the saccadic burst cells present in SC (Munoz & Wurtz, 1993a, 1993b, 1995a, 1995b). These have a burst of activity before a saccade and are quite silent during fixation and saccade preparation periods. Burst cell activities b_{ij} obey the equation:

$$\frac{db_{ij}}{dt} = -20b_{ij} + (1.2 - b_{ij})B_{ij}^E - (1 + b_{ij})B_{ij}^I, \quad (30)$$

where the excitatory input equals:

$$B_{ij}^E = 8r_{ij} + 30f(u_{ij}) + 155.0[f_{ij}^O]^+ \quad (31)$$

SC burst cells receive excitatory input from the retina (r_{ij}), from buildup cells (u_{ij} , see equation (35)) and from the output layer of the FEF (f_{ij}^O , see equation (54)). The sigmoidal signal function ($f(u_{ij})$) is defined as:

$$f(x) = \frac{x^3}{x^3 + 0.07^3}. \quad (32)$$

The SC burst cell inhibitory input equals:

$$B_{ij}^I = 10M + 70[u_{ff}]^+ + 110n(n_{ij}). \quad (33)$$

These cells are inhibited by the mesencephalic reticular formation (M , see equation (46)), the fixation cell (u_{ff} , see equation (42)) and by the substantia nigra ($n(n_{ij})$, see equation (47)). The sigmoidal function ($n(x)$) is defined as:

$$n(x) = \frac{x^3}{x^3 + 0.4^3}. \quad (34)$$

SC Buildup Cells. Model buildup cells mimic the SC buildup cells in SC. They have no activity during fixation and show sustained buildup activity during the saccade preparation phase followed by a burst of activity prior to saccade initiation. The activities of the SC buildup cell layer (u_{ij}) obey the equation:

$$\frac{du_{ij}}{dt} = -0.1u_{ij} + (1 - u_{ij})U_{ij}^E - u_{ij}U_{ij}^I. \quad (35)$$

The excitatory input to SC buildup cells (U_{ij}^E) is given by:

$$U_{ij}^E = r_{ij} + 5[f_{ij}^I]^+ + [a_{ij}]^+ + 40c(u_{ij}) + 4 \sum_l \sum_k g(b_{lk} H_{k-j} H_{l-i}), \quad (36)$$

where

$$g(x) = 0.035x^{0.65}. \quad (37)$$

SC buildup cells are excited by the retina (r_{ij}), the planning layer of the FEF (f_{ij}^I , see equation (48)), the parietal cortex (a_{ij} , see equation (59)), and via self-excitatory connections ($c(u_{ij})$), and by the burst cell layer (b_{lk}). The self-excitatory feedback signal is threshold-linear:

$$c(x) = [x - 0.035]^+. \quad (38)$$

The spread of input from the burst layer to buildup layer is a Gaussian described by:

$$H_i = 100e^{-i^2}. \quad (39)$$

The inhibitory input to SC buildup cells (U_{ij}^I) is given by:

$$U_{ij}^I = 40M + 0.8[u_{ff}]^+ + 8n(n_{ij}) + \sum_{\substack{l=j+6 \\ l \neq j}}^{l=j+6} \sum_{\substack{k=i+6 \\ k \neq i}}^{k=i+6} c(u_{kl})M_{k-i}M_{l-j}. \quad (40)$$

Inhibition comes from the mesencephalic formation (term M), the fixation cell (u_{ff}), the substantia nigra ($n(n_{ij})$), and other buildup cells ($c(u_{kl})$). There is strong mutual inhibition between buildup cells. The strength (M_i) of this inhibition is a Gaussian function of distance:

$$M_i = e^{-0.02i^2}. \quad (41)$$

SC Fixation Cells. Fixation cells are active during fixation and become silent during saccades. Model SC fixation cells obey:

$$\frac{du_{ff}}{dt} = -0.1u_{ff} + (0.1 - u_{ff})(10\zeta + r_{00} + K^E) - u_{ff} \left(10 \sum_{\substack{k=1 \\ k \neq f}}^N \sum_{\substack{j=1 \\ j \neq f}}^N u_{kj} M_j M_k + 10 \sum_{\substack{k=1 \\ k \neq f}}^N \sum_{\substack{j=1 \\ j \neq f}}^N b_{kj} \right). \quad (42)$$

The fixation cell activity (u_{ff}) is excited by a fixation signal (term ζ), defined as:

$$\zeta = \begin{cases} 1.0 & \text{if } t < T_{fix} \quad (T_{fix} \text{ is the time at which fixation light goes off}) \\ 0 & \text{otherwise} \end{cases}. \quad (43)$$

It is also excited by visual input from the fovea (r_{00}) and MT cells (K^E , see simulation 1) whose receptive fields contain the fovea, defined by:

$$K^E = \sum_{ij \in F_\delta} m_{ij}^- \quad \text{where } F_\delta = \left\{ (i, j) \text{ such that } f - \delta \leq i \leq f + \delta \right. \\ \left. \text{and } f - \delta \leq j \leq f + \delta \right\}. \quad (44)$$

In (44), δ is the radius of response field of the MT cell at position (i, j) , and f indicates the position of the fovea.

Activity in buildup cells (term u_{kj}) or burst cells (term b_{kj}) inhibits fixation cell activity. As a result, once a saccade is initiated, fixation cells go silent. Since buildup layer cells are involved in saccade planning as well as saccade execution, both buildup and fixation cell activity can co-exist. This property is realized by using a distance-dependent Gaussian inhibition from

buildup cells to fixation cells (term $10 \sum_{k=2}^N \sum_{j=2}^N u_{kj} M_j M_k$). The buildup inhibitory kernel equals:

$$M_i = 0.1e^{-0.01i^2}. \quad (45)$$

MRF Cells. The mesencephalic reticular formation input in equations (33) and (40) is defined by:

$$M = \begin{cases} 1 & \text{if } \sum_{i, j \neq \text{fovea}}^N u_{ij} > 0 \\ 0 & \text{otherwise} \end{cases}. \quad (46)$$

It is active if there is any activity in the nonfoveal part of SC buildup cell layer (u_{ij}).

SNr Cell. Cell activity (n_{ij}) in the model substantia nigra follows the equation:

$$\frac{dn_{ij}}{dt} = (1 - n_{ij})(1.7 + 200\zeta) - 2(1 + n_{ij})n_{ij}f_{ij}^I. \quad (47)$$

It is excited by a constant arousal signal (term 1.7) and by the fixation signal (ζ , see equation (43)). The nigral cells are inhibited by the FEF planning layer cells (f_{ij}^I , see equation (48)).

FEF Cells: The model's frontal eye field is comprised of two cell layers or maps: FEF planning cells and output cells.

FEF planning layer cells. The FEF planning layer cells are involved in saccadic planning and execution. Reciprocal connections with LIP help these cells achieve target selection in a stimulus rich environment. The equations for planning cell activity f_{ij}^I at each position (i, j) is a simplified representation of a similar equation in Brown et al. (Brown et al., 2004):

$$\frac{df_{ij}^I}{dt} = (1 - f_{ij}^I)F_{ij}^{PE} - (f_{ij}^I + 0.4)F_{ij}^{PI}, \quad (48)$$

where the excitatory input (F_{ij}^{PE}) obeys:

$$F_{ij}^{PE} = 10[a_{ij}]^+ + 15I_{ij} + 1.5[g^S - 0.5]^+ + 2f(f_{ij}^I). \quad (49)$$

Each planning layer cell at position (i, j) receive excitatory input from the parietal cortex (a_{ij}), and from a smoothed retinal input (I_{ij}) defined as:

$$I_{ij} = \sum_{(p,q) \in \Psi} R_{ij} \exp\left(\frac{-(p-i)^2 - (q-j)^2}{0.7^2}\right), \quad (50)$$

where Ψ is the set of eight nearest neighbors in cartesian input space. Additional excitatory input in equation (49) comes from the decision variable ($[g^S - 0.5]^+$) and via a self-excitatory recurrent on-center (term $2f(f_{ij}^I)$). When the decision signal (g^S) goes over 0.5, it boosts the activity of all active neurons. This additional excitation gets amplified by the self-excitatory loop. That is, this combination ensures that the maximally active neuron gets the biggest boost in activity compared to the rest of the neurons. Thus, this combination realizes a target selection network among the planning layer neurons. The sigmoidal signal function ($f(x)$) controlling the FEF planning cell input is defined as:

$$f(x) = \frac{([x]^+)^8}{([x]^+)^8 + 0.5^8}. \quad (51)$$

The inhibitory input to equation (48) obeys:

$$F_{ij}^{PI} = 0.8 + 10([f_{ff}^I]^+ e^{-((i-f)^2 + (j-f)^2)}) + 20 \sum_{\substack{r \neq i \\ s \neq j}} f_{rs}^I + 10S_{on}. \quad (52)$$

In (52), each planning layer cell receives a distance-dependent inhibition from the FEF fixation cell (term f_{ff}^I), and from other active FEF planning cells via recurrent inhibition ($20 \sum_{\substack{r \neq i \\ s \neq j}} f_{rs}^I$).

These cells also get strong inhibition after saccade initiation in the form of “*saccade on*” signal (S_{on}). This signal takes the value 1 only if a saccade is underway and is zero during the rest of the interval. This might be thought of as FEF post-saccadic cell input.

FEF fixation cell. f_{ff}^I is the activity of the FEF fixation cell that is analogous to the SC fixation cell. It obeys the equation:

$$\frac{df_{ff}^I}{dt} = -0.1f_{ff}^I + (1 - f_{ff}^I)(10\zeta + r_{00}) - (1 + f_{ff}^I)F_{ff}^I. \quad (53)$$

This cell receives excitatory input from the fovea (r_{00}) and from the fixation input (ζ , described in equation (43)). The inhibitory input to the fixation cells obeys:

$$F_{ff}^I = 0.1 \sum_{ij} (f_{ij}^I e^{-0.01((i-f)^2 + (j-f)^2)} + f_{ij}^O). \quad (54)$$

FEF fixation cells are inhibited by the FEF input cells (f_{ij}^I) and output cells (f_{ij}^O), much like the SC fixation cells.

FEF Output cells. Model FEF output cells correspond to FEF movement or presaccadic cells. They convey the saccadic choice to SC and to the saccade generator in brainstem and thereby help execute a saccade. Their activities are defined by:

$$\frac{df_{ij}^O}{dt} = (1 - f_{ij}^O)F_{ij}^{OE} - (f_{ij}^O + 0.8)F_{ij}^{OI}. \quad (55)$$

In (55), the excitatory input F_{ij}^{OE} obeys the equation:

$$F_{ij}^{OE} = 0.4[f_{ij}^I - 0.2]^+ + 5[a_{ij}]^+ + 1.5[g^S - 0.5]^+. \quad (56)$$

Excitatory inputs come from FEF input cells ($0.4[f_{ij}^I - 0.2]^+$) and parietal cells ($5a_{ij}$), but their suprathreshold activation strongly depends on excitation by the decision signal ($1.5[g^S - 0.5]^+$).

The inhibitory input F_{ij}^{OI} in equation (55) obeys:

$$F_{ij}^{OI} = 20 \sum_{\substack{p \neq i \\ q \neq j}} f_{pq}^O, \quad (57)$$

which provides strong mutual inhibition from other FEF output cells ($20 \sum_{\substack{p \neq i \\ q \neq j}} f_{pq}^O$). This strong mutual inhibition ensures that only the maximally active cell in the planning layer goes on to become a motor output, i.e., to generate a saccade.

Decision Signal. The decision variable g^S , which is meant to represent the results of a competitive choice by a cortico-(basal ganglia)-thalamo-cortical loop (see in Brown et al., 2004):

$$\frac{dg^S}{dt} = -0.6g^S + 20(1 - g^S) \left(\sum_{ij} ([f_{ij}^I - 0.33]^+ + [a_{ij} - 0.6]^+ + [u_{ij} - 0.2]^+) \right). \quad (58)$$

In (58), activity g^S is maximal when there are synchronous inputs from all the three retinotopically in-register areas namely: FEF planning layer cells (f_{ij}^I), LIP visual cells (a_{ij}), and SC buildup cells (u_{ij}). Higher values of g^S enable faster target selection.

PPC Cells. Parietal cortex cell activities (a_{ij}) represent the responses in the lateral bank of intra-parietal area (LIP), which code visual stimuli in motor error coordinates. They receive retinal and FEF input and project back to the FEF. They are modeled as:

$$\frac{da_{ij}}{dt} = (1 - a_{ij})[I_{ij} + [f_{ij}^I]^+ + f(f_{ij}^O) + f(a_{ij})] - a_{ij} \left[20 \sum_{\substack{x \neq i \\ y \neq j}} [a_{xy}]^+ + a_{ij}^R \right]. \quad (59)$$

The excitatory input consists of a smoothed retinal input (I_{ij} , see equation (50)), FEF planning cells (f_{ij}^I), FEF output cells ($f(f_{ij}^O)$), and recurrent on-center connections ($f(a_{ij})$). The parameters for the sigmoidal signal function ($f(x)$, in equation (59)) were chosen such that there is sustained activity even during the delay period of the delayed-saccade paradigm. It is described as:

$$f(x) = \frac{x^7}{x^7 + 0.4^7}. \quad (60)$$

The inhibitory input to these cells consists of recurrent off-surround connections ($20 \sum_{\substack{x \neq i \\ y \neq j}} [a_{xy}]^+$)

and a more slowly varying recurrent self-inhibition (a_{ij}^R , see equation (61)). Dynamics for the interneuron-mediated self-inhibition obey:

$$\frac{da_{ij}^R}{dt} = (1 - a_{ij}^R)a_{ij} - a_{ij}^R. \quad (61)$$

These inhibitory connections replicate the slow decay of delay-period activity observed in primate parietal cells when the animal was doing a delayed saccade.

CBM cells: SC burst cells (b_{ij}) and FEF output cells (f_{ij}^O) activate cerebellar cells that control the learning of eye movement gains. The SC-activated cerebellar cell activities (c_{ij}^S) obey:

$$\frac{dc_{ij}^S}{dt} = -0.1c_{ij}^S + (1 - c_{ij}^S)r(b_{ij}) - 6(c_{ij}^S + 0.05) \sum_{i,j=1}^N o(c_{ij}^F). \quad (62)$$

Here, excitatory input comes from SC burst cells ($r(b_{ij})$) and inhibition from all cerebellar FEF-activated cells ($-\sum_{i,j=1}^N o(c_{ij}^F)$). Similarly, FEF-activated cells activities (c_{ij}^F) obey:

$$\frac{dc_{ij}^F}{dt} = -0.1c_{ij}^F + (1 - c_{ij}^F)r(f_{ij}^O) - (c_{ij}^F + 0.05) \sum_{i,j=1}^N o(c_{ij}^S). \quad (63)$$

These cells are excited by the output layer of FEF ($r(f_{ij}^O)$) and inhibited by all the cerebellar SC cells ($-\sum_{i,j=1}^N o(c_{ij}^S)$). The SC and FEF cerebellar cells hereby inhibit each other and compete for dominance (Gancarz and Grossberg, 1999). The excitatory signal function ($r(x)$, in equations (62) & (63)) is defined by:

$$r(x) = \frac{x^4}{x^4 + 0.2^4}. \quad (64)$$

The inhibitory sigmoidal function ($o(x)$, in equations (62) & (63)) given by:

$$o(x) = \frac{x^2}{x^2 + 0.5^2}. \quad (65)$$

Using the same excitatory and inhibitory sigmoidal functions for SC-activated and FEF-activated cerebellar cells biases the network such that that FEF activity gets more preference if the maximal activities of FEF output cells and SC burst cells are out of sync. That is, the output

saccade vector will not be a vector average, but will be more biased towards the vector represented by the maximally active FEF output cell.

Cerebellar learning corrects movement errors via adaptive gain control. For example, if the saccadic target was at position $(10^\circ, 10^\circ)$ and the saccade landed the eye at $(9^\circ, 11^\circ)$ from its original position, then the retinotopic error is $(1^\circ, -1^\circ)$. The error B_θ , where $\theta = 0^\circ, 90^\circ, 180^\circ$, or 270° , is calculated by breaking the retinotopic location into its constituent horizontal and vertical components. Thus the error takes the values: $B_{0^\circ} = 1$, $B_{90^\circ} = -1$, $B_{180^\circ} = 0$ and $B_{270^\circ} = 0$ when the eye foveates after moving 9° to right and 11° upwards. Learning is triggered in the cerebellum by the error-driven teaching signals γ_θ , and is given by:

$$\gamma_\theta = B_\theta. \quad (66)$$

The teaching signal is on for just a single integration step. The adaptive weights learn when both the teaching and the sampling signals are present. Opponent learning ($\gamma_\theta - \gamma_\ominus$) allows weights to either increase or decrease and thus correct saccadic undershoots or overshoots (Grossberg and Kuperstein, 1986). The learning rules for weights mediating the FEF-activated cells (W_{ij}^F), SC-activated cerebellar cells (W_{ij}^S) and DLPN cells (W_{ij}^D) are given by:

$$\frac{dW_{ij}^S}{dt} = 67.5c_{ij}^S(\gamma_\theta - \gamma_\ominus), \quad (67)$$

$$\frac{dW_{ij}^F}{dt} = 67.5c_{ij}^F(\gamma_\theta - \gamma_\ominus), \quad (68)$$

$$\frac{dW_{vd}^D}{dt} = 67.5p_{vd}^D(\gamma_\theta - \gamma_\ominus), \quad (69)$$

PPRF Cells: Equations defining saccade generator cell activities are similar to equations present in Gancarz and Grossberg (1999). The saccadic drive (I_θ^S) is calculated by adding direct SC input with the cerebellar input and is described by:

$$I_\theta^S = 120 \left(\sum_{j=1}^N \sum_{i=1}^N (c_{ij}^S W_{ij}^S + c_{ij}^F W_{ij}^F) + \sum_d \sum_v p_{vd}^D W_{vd}^D + 4K^B + 4K^U \right). \quad (70)$$

Saccadic input from the cerebellum is the sum of all weighed activities of FEF (c_{ij}^F), SC (c_{ij}^S) and DLPN (p_{vd}^D) signals. The direct projections from the SC burst cells (K^B) and SC buildup layers (K^U) pass through sigmoidal transfer functions defined by equation (71) and (72), respectively:

$$K^B = \frac{b_{ij}^3}{0.4^3 + b_{ij}^3} \quad (71)$$

and

$$K^U = \frac{u_{ij}^3}{0.1^3 + u_{ij}^3}. \quad (72)$$

The turning points (0.4 and 0.1) of the sigmoidal functions (K^B and K^U) were chosen so that, in case FEF is lesioned, there will be enough drive from SC to initiate a saccade.

Long lead burst neurons (LLBNs): LLBNs form the input stage for the saccade generator. They receive input from the cerebellum and from SC burst and buildup neurons (Rodgers et al.,

2006). They provide accelerate and brake signals needed for saccade initiation and termination. The LLBN activities (l_θ) obey the equation:

$$\frac{dl_\theta}{dt} = -1.3l_\theta + I_\theta^S - 2I_\Theta^S - 2b_\theta. \quad (73)$$

In (73), Θ indicates the opposite direction and is defined as $\Theta = \theta + 180$.

The LLBN activity follows a push-pull opponent mechanism. It is excited by saccadic drive along its preferred direction (I_θ^S) and is inhibited by both the saccadic drive along the opponent direction ($2I_\Theta^S$) and by the inhibitory burst neurons (term $2b_\theta$, see equation (75)). Stronger coefficients for the inhibitory inputs ($2I_\Theta^S$ and $2b_\theta$, twice the excitatory input I_θ^S) are needed to achieve fast and accurate braking and thereby help in saccade termination.

Excitatory burst neurons (EBNs): EBNs receive input from LLBNs and are inhibited by the OPNs. As long as EBNs are active, the eye keeps moving. EBN cell activities (e_θ) are modeled as:

$$\frac{de_\theta}{dt} = -3.5e_\theta + (2 - e_\theta)(5l_\theta + 1) - (1 + e_\theta)(2l_\Theta + 20v(o)). \quad (74)$$

Excitatory input comes from the agonistic LLBNs (l_θ) as well as an arousal signal (set equal to 1). Antagonistic LLBNs (l_Θ) and OPNs ($v(o)$, see equation (28)) inhibit the cell.

Inhibitory burst neurons (IBNs): IBN cell activities (b_θ) form a negative feedback loop that controls the amplitude and duration of LLBN activity. They obey the equation:

$$\frac{db_\theta}{dt} = -15b_\theta + 50e_\theta. \quad (75)$$

The Inhibitory burst neurons are excited by the agonistic EBNs (e_θ) and send inhibitory feedback to the agonistic LLBNs (l_θ , equation (73)).

Tonic Neurons: Tonic neurons integrate the EBN burst (e_θ) and pursuit (h_θ) cell outputs via push-pull opponent organization:

$$\frac{dt_\theta}{dt} = 0.3(e_\theta - e_\Theta) + 0.15(h_\theta - h_\Theta). \quad (76)$$

Eye position (Ψ) is changed using the following formula:

$$\Psi = 20(t_\theta - t_\Theta). \quad (77)$$

Opponency ($t_\theta - t_\Theta$) allows the eye to change its direction smoothly while tracking a target which makes sudden changes in its direction of motion.

References

- Adler, S. A., Bala, J., & Krauzlis, R. J. (2002). Primacy of spatial information in guiding target selection for pursuit and saccades. *J Vis*, 2(9), 627-644.
- Albright, T. D. (1984). Direction and orientation selectivity of neurons in visual area MT of the macaque. *J Neurophysiol*, 52(6), 1106-1130.
- Arai, K., McPeck, R. M., & Keller, E. L. (2004). Properties of Saccadic Responses in Monkey When Multiple Competing Visual Stimuli Are Present. *J Neurophysiol*, 91(2), 890-900.
- Basso, M. A., Krauzlis, R. J., & Wurtz, R. H. (2000). Activation and inactivation of rostral superior colliculus neurons during smooth-pursuit eye movements in monkeys. *J Neurophysiol*, 84(2), 892-908.
- Basso, M. A., & Wurtz, R. H. (2002). Neuronal Activity in Substantia Nigra Pars Reticulata during Target Selection. *J. Neurosci.*, 22(5), 1883-1894.
- Belknap, D. B., & Noda, H. (1987). Eye movements evoked by microstimulation in the flocculus of the alert macaque. *Exp Brain Res*, 67(2), 352-362.
- Brodal, P. (1980). The cortical projection to the nucleus reticularis tegmenti pontis in the rhesus monkey. *Exp Brain Res*, 38(1), 19-27.
- Brown, J. W., Bullock, D., & Grossberg, S. (2004). How laminar frontal cortex and basal ganglia circuits interact to control planned and reactive saccades. *Neural Netw*, 17(4), 471-510.
- Butler, A. B., & Hodos, W. (1996). Comparative vertebrate neuroanatomy. New York: Wiley-Liss
- Büttner U., Büttner-Ennever J.A. (1989). Present concepts of oculomotor organization. *Rev Oculomot Res*. 2, 3-32.
- Büttner-Ennever J.A., Horn A.K., Henn, V., Cohen, B.(1999). Projections from the superior colliculus motor map to omnipause neurons in monkey. *J. Comp. Neurol*, 413(1), 55-67
- Büttner U., Büttner-Ennever J.A. (2005). Present concepts of oculomotor organization. *Prog Brain Res*. 151, 1-42.
- Carello, C. D., & Krauzlis, R. J. (2004). Manipulating intent: evidence for a causal role of the superior colliculus in target selection. *Neuron*, 43(4), 575-583.
- Carey, M. R., & Lisberger, S. G. (2004). Signals that modulate gain control for smooth pursuit eye movements in monkeys. *J Neurophysiol*, 91(2), 623-631.
- Carpenter, G. A., & Grossberg, S. (1993). Normal and amnesic learning, recognition and memory by a neural model of cortico-hippocampal interactions. *Trends Neurosci*, 16(4), 131-137.
- Case, G. R., & Ferrera, V. P. (2007). Coordination of smooth pursuit and saccadic target selection in monkeys. *J Neurophysiol*, 98(4), 2206-2214.
- Clower, D. M., West, R. A., Lynch, J. C., & Strick, P. L. (2001). The inferior parietal lobule is the target of output from the superior colliculus, hippocampus, and cerebellum. *J Neurosci*, 21(16), 6283-6291.
- Collins, C. E., Lyon, D. C., & Kaas, J. H. (2005). Distribution across cortical areas of neurons projecting to the superior colliculus in new world monkeys. *Anat Rec A Discov Mol Cell Evol Biol*, 285(1), 619-627.
- Cui, D. M., Yan, Y. J., & Lynch, J. C. (2003). Pursuit subregion of the frontal eye field projects to the caudate nucleus in monkeys. *J Neurophysiol*, 89(5), 2678-2684.
- Davidson, R. M., & Bender, D. B. (1991). Selectivity for relative motion in the monkey superior colliculus. *J Neurophysiol*, 65(5), 1115-1133.

- Everling, S., Pare, M., Dorris, M. C., & Munoz, D. P. (1998). Comparison of the discharge characteristics of brain stem omnipause neurons and superior colliculus fixation neurons in monkey: implications for control of fixation and saccade behavior. *J Neurophysiol*, 79(2), 511-528.
- Ferrera, V. P., & Lisberger, S. G. (1995). Attention and target selection for smooth pursuit eye movements. *J Neurosci*, 15(11), 7472-7484.
- Fuchs A.F., Kaneko C.R., Scudder C.A. (1985). Brainstem control of saccadic eye movements. *Annu Rev Neurosci*. 8, 307-37
- Gancarz, G., & Grossberg, S. (1999). A neural model of saccadic eye movement control explains task-specific adaptation. *Vision Res*, 39(18), 3123-3143.
- Gandhi, N. J., & Keller, E. L. (1997). Spatial distribution and discharge characteristics of superior colliculus neurons antidromically activated from the omnipause region in monkey. *J Neurophysiol*, 78(4), 2221-2225.
- Garbutt, S., & Lisberger, S. G. (2006). Directional Cuing of Target Choice in Human Smooth Pursuit Eye Movements. *J Neurosci*, 26(48), 12479-12486.
- Gardner, J. L., & Lisberger, S. G. (2001). Linked target selection for saccadic and smooth pursuit eye movements. *J Neurosci*, 21(6), 2075-2084.
- Gardner, J. L., & Lisberger, S. G. (2002). Serial linkage of target selection for orienting and tracking eye movements. *Nat Neurosci*, 5(9), 892-899.
- Girard B., Berthoz A. (2005) From brainstem to cortex: computational models of saccade generation circuitry. *Prog Neurobiol*. 77(4), 215-51
- Giolli, R. A., Gregory, K. M., Suzuki, D. A., Blanks, R. H., Lui, F., & Betelak, K. F. (2001). Cortical and subcortical afferents to the nucleus reticularis tegmenti pontis and basal pontine nuclei in the macaque monkey. *Vis Neurosci*, 18(5), 725-740.
- Gold, J. I., & Shadlen, M. N. (2000). Representation of a perceptual decision in developing oculomotor commands. *Nature*, 404(6776), 390-394.
- Gold, J. I., & Shadlen, M. N. (2001). Neural computations that underlie decisions about sensory stimuli. *Trends Cogn Sci*, 5(1), 10-16.
- Gottlieb, J. P., Bruce, C. J., & MacAvoy, M. G. (1993). Smooth eye movements elicited by microstimulation in the primate frontal eye field. *J Neurophysiol*, 69(3), 786-799.
- Grossberg, S. (1973). Contour enhancement, short-term memory, and constancies in reverberating neural networks. *Studies in Applied Mathematics*, 52, 213-257.
- Grossberg, S. (1980). Biological competition: Decision rules, pattern formation, and oscillations. *Proc Natl Acad Sci U S A*, 77(4), 2338-2342.
- Grossberg, S. (1982). *Studies of mind and brain*. Amsterdam:: Kluwer/Reidel.
- Grossberg, S. (2000). The complementary brain: unifying brain dynamics and modularity. *Trends Cogn Sci*, 4(6), 233-246.
- Grossberg, S. (2003). How Does the Cerebral Cortex Work? Development, Learning, Attention, and 3-D Vision by Laminar Circuits of Visual Cortex. *Behav and Cogn Neurosci Revs*, 2, 47-76.
- Grossberg, S., Mingolla, E., & Pack, C. (1999). A neural model of motion processing and visual navigation by cortical area MST. *Cereb Cortex*, 9(8), 878-895.
- Grossberg, S., & Pilly, P. Y. (2008). Temporal dynamics of decision making during motion perception in the visual cortex. *Vis Res*, *in press*.

- Grossberg, S., Roberts, K., Aguilar, M., & Bullock, D. (1997). A neural model of multimodal adaptive saccadic eye movement control by superior colliculus. *J Neurosci*, *17*(24), 9706-9725.
- Grossberg, S., Srihasam, K., & Bullock, D. (2007). Neural dynamics of saccadic and smooth pursuit eye movement coordination during visual tracking of unpredictably moving targets. *Technical Report BU CAS/CNS TR-07-018*, Submitted for Publication.
- Hikosaka, O., & Wurtz, R. H. (1983). Visual and oculomotor functions of monkey substantia nigra pars reticulata. IV. Relation of substantia nigra to superior colliculus. *J Neurophysiol*, *49*(5), 1285–1301.
- Hodgkin, A. L. (1964). The Ionic Basis of Nervous Conduction. *Science*, *145*, 1148-1154.
- Horwitz, G. D., & Newsome, W. T. (2001). Target selection for saccadic eye movements: direction-selective visual responses in the superior colliculus. *J Neurophysiol*, *86*(5), 2527-2542.
- Huerta, M. F., Krubitzer, L. A., & Kaas, J. H. (1987). Frontal eye field as defined by intracortical microstimulation in squirrel monkeys, owl monkeys, and macaque monkeys. II. Cortical connections. *J Comp Neurol*, *265*(3), 332-361.
- Keating, E. G., Pierre, A., & Chopra, S. (1996). Ablation of the pursuit area in the frontal cortex of the primate degrades foveal but not optokinetic smooth eye movements. *J Neurophysiol*, *76*(1), 637-641.
- Komatsu, H., & Wurtz, R. H. (1989). Modulation of pursuit eye movements by stimulation of cortical areas MT and MST. *J Neurophysiol*, *62*(1), 31-47.
- Krauzlis, R. J. (2005). The control of voluntary eye movements: new perspectives. *Neuroscientist*, *11*(2), 124-137.
- Krauzlis, R. J., Basso, M. A., & Wurtz, R. H. (1997). Shared Motor Error for Multiple Eye Movements. *Science*, *276*(5319), 1693-1695.
- Krauzlis, R. J., Basso, M. A., & Wurtz, R. H. (2000). Discharge properties of neurons in the rostral superior colliculus of the monkey during smooth-pursuit eye movements. *J Neurophysiol*, *84*(2), 876-891.
- Krauzlis, R. J., Liston, D., & Carello, C. D. (2004). Target selection and the superior colliculus: goals, choices and hypotheses. *Vision Res*, *44*(12), 1445-1451.
- Krauzlis, R. J., Zivotofsky, A. Z., & Miles, F. A. (1999). Target selection for pursuit and saccadic eye movements in humans. *J Cogn Neurosci*, *11*(6), 641-649.
- Lo, C.C., & Wang X.J. (2006). Cortico-basal ganglia circuit mechanism for a decision threshold in reaction time tasks. *Nat Neurosci*, *9*(7), 956-63
- Lynch, J. C., Graybiel, A. M., & Lobeck, L. J. (1985). The differential projection of two cytoarchitectonic subregions of the inferior parietal lobule of macaque upon the deep layers of the superior colliculus. *J Comp Neurol*, *235*(2), 241-254.
- Lynch, J. C., & Tian, J. R. (2005). Cortico-cortical networks and cortico-subcortical loops for the higher control of eye movements. *Prog Brain Res*, *151*, 461-501.
- Maioli, M. G., Domeniconi, R., Squatrito, S., & Riva Sanseverino, E. (1992). Projections from cortical visual areas of the superior temporal sulcus to the superior colliculus, in macaque monkeys. *Arch Ital Biol*, *130*(3), 157-166.
- Martin, K. E., Phillips, J. G., & Iansek, R. (1994). Inaccuracy and instability of sequential movements in Parkinson's disease. *Exp Brain Res*, *102*, 131–140.

- Maunsell, J. H., & van Essen, D. C. (1983a). The connections of the middle temporal visual area (MT) and their relationship to a cortical hierarchy in the macaque monkey. *J Neurosci*, 3(12), 2563-2586.
- Maunsell, J. H., & Van Essen, D. C. (1983b). Functional properties of neurons in middle temporal visual area of the macaque monkey. I. Selectivity for stimulus direction, speed, and orientation. *J Neurophysiol*, 49(5), 1127-1147.
- McPeck, R. M., & Keller, E. L. (2002). Saccade Target Selection in the Superior Colliculus During a Visual Search Task. *J Neurophysiol*, 88(4), 2019-2034.
- McPeck R. M., Keller E. L. (2004) Deficits in saccade target selection after inactivation of superior colliculus. *Nat Neurosci*. 7(7), 757-63.
- Missal, M., & Keller, E. L. (2002). Common inhibitory mechanism for saccades and smooth-pursuit eye movements. *J Neurophysiol*, 88(4), 1880-1892.
- Moschovakis A.K., Highstein S.M. (1994). The anatomy and physiology of primate neurons that control rapid eye movements. *Annu Rev Neurosci*. 17, 465-88
- Munoz, D. P., Dorris, M. C., Pare, M., & Everling, S. (2000). On your mark, get set: brainstem circuitry underlying saccadic initiation. *Can J Physiol Pharmacol*, 78(11), 934-944.
- Munoz, D. P., & Wurtz, R. H. (1993a). Fixation cells in monkey superior colliculus. I. Characteristics of cell discharge. *J Neurophysiol*, 70(2), 559-575.
- Munoz, D. P., & Wurtz, R. H. (1993b). Fixation cells in monkey superior colliculus. II. Reversible activation and deactivation. *J Neurophysiol*, 70(2), 576-589.
- Munoz, D. P., & Wurtz, R. H. (1995a). Saccade-related activity in monkey superior colliculus. I. Characteristics of burst and buildup cells. *J Neurophysiol*, 73(6), 2313-2333.
- Munoz, D. P., & Wurtz, R. H. (1995b). Saccade-related activity in monkey superior colliculus. II. Spread of activity during saccades. *J Neurophysiol*, 73(6), 2334-2348.
- Mustari, M. J., Fuchs, A. F., & Wallman, J. (1988). Response properties of dorsolateral pontine units during smooth pursuit in the rhesus macaque. *J Neurophysiol*, 60(2), 664-686.
- Ono, S., Das, V. E., Economides, J. R., & Mustari, M. J. (2005). Modeling of smooth pursuit-related neuronal responses in the DLPN and NRTP of the rhesus macaque. *J Neurophysiol*, 93(1), 108-116.
- Ono, S., Das, V. E., & Mustari, M. J. (2004). Gaze-related response properties of DLPN and NRTP neurons in the rhesus macaque. *J Neurophysiol*, 91(6), 2484-2500.
- Ottes, F. P., Van Gisbergen, J. A., & Eggermont, J. J. (1984). Metrics of saccade responses to visual double stimuli: two different modes. *Vision Res*, 24(10), 1169-1179.
- Pack, C., Grossberg, S., & Mingolla, E. (2001). A neural model of smooth pursuit control and motion perception by cortical area MST. *J Cogn Neurosci*, 13(1), 102-120.
- Pare, M., & Guitton, D. (1994). The fixation area of the cat superior colliculus: effects of electrical stimulation and direct connection with brainstem omnipause neurons. *Exp Brain Res*, 101(1), 109-122.
- Passingham, R. (1993). *The frontal lobes and voluntary action*. Oxford: Oxford University Press.
- Recanzone, G. H., & Wurtz, R. H. (1999). Shift in smooth pursuit initiation and MT and MST neuronal activity under different stimulus conditions. *J Neurophysiol*, 82(4), 1710-1727.
- Rodgers, C.K., Munoz, D.P., Scott, S.H., & Paré, M. (2006). Discharge properties of monkey tectoreticular neurons. *J Neurophysiol*, 95(6), 3502-11.
- Roitman, J. D., & Shadlen, M. N. (2002). Response of neurons in the lateral intraparietal area during a combined visual discrimination reaction time task. *J Neurosci*, 22(21), 9475-9489.

- Schall, J. D., Hanes, D. P., Thompson, K. G., & King, D. J. (1995). Saccade target selection in frontal eye field of macaque. I. Visual and premovement activation. *J. Neurosci.*, *15*(10), 6905-6918.
- Schall, J. D., Morel, A., King, D. J., & Bullier, J. (1995). Topography of visual cortex connections with frontal eye field in macaque: convergence and segregation of processing streams. *J Neurosci*, *15*(6), 4464-4487.
- Schall, J. D., & Thompson, K. G. (1999). Neural selection and control of visually guided eye movements. *Annual Review of Neuroscience*, *22*(1), 241-259.
- Schiller, P. H., & Chou, I. H. (1998). The effects of frontal eye field and dorsomedial frontal cortex lesions on visually guided eye movements. *Nat Neurosci*, *1*(3), 248-253.
- Schiller, P. H., & Tehovnik, E. J. (2001). Look and see: how the brain moves your eyes about. *Prog Brain Res*, *134*, 127-142.
- Schiller, P. H., & Tehovnik, E. J. (2003). Cortical inhibitory circuits in eye-movement generation. *Eur J Neurosci*, *18*(11), 3127-3133.
- Schiller, P. H., & Tehovnik, E. J. (2005). Neural mechanisms underlying target selection with saccadic eye movements. *Prog Brain Res*, *149*, 157-171.
- Seidemann, E., & Newsome, W. T. (1999). Effect of spatial attention on the responses of area MT neurons. *J Neurophysiol*, *81*(4), 1783-1794.
- Shadlen, M. N., & Newsome, W. T. (2001). Neural basis of a perceptual decision in the parietal cortex (area LIP) of the rhesus monkey. *J Neurophysiol*, *86*(4), 1916-1936.
- Shi, D., Friedman, H. R., & Bruce, C. J. (1998). Deficits in smooth-pursuit eye movements after muscimol inactivation within the primate's frontal eye field. *J Neurophysiol*, *80*(1), 458-464.
- Sommer, M. A., & Wurtz, R. H. (2000). Composition and topographic organization of signals sent from the frontal eye field to the superior colliculus. *J Neurophysiol*, *83*(4), 1979-2001.
- Sommer, M. A., & Wurtz, R. H. (2004). What the brain stem tells the frontal cortex. I. Oculomotor signals sent from superior colliculus to frontal eye field via mediodorsal thalamus. *J Neurophysiol*, *91*(3), 1381-1402.
- Spatz, W. B., & Tigges, J. (1973). Studies on the visual area MT in primates. II. Projection fibers to subcortical structures. *Brain Res*, *61*, 374-378.
- Stanton, G.B., Goldberg, M.E., & Bruce, C.J. (1988). Frontal eye field efferents in the macaque monkey: II. Topography of terminal fields in midbrain and pons. *J Comp Neurol*, *271*(4), 493-506.
- Strick, P. L., Dum, R. P., & Picard, N. (1995). Macro-organization of the circuits connecting the basal ganglia with the cortical motor areas. In J. Houk, J. Davis, & D. Beiser (Eds.), *Models of information processing in the basal ganglia* (pp. 117-130). Cambridge: MIT Press.
- Suzuki, D. A., & Keller, E. L. (1984). Visual signals in the dorsolateral pontine nucleus of the alert monkey: their relationship to smooth-pursuit eye movements. *Exp Brain Res*, *53*(2), 473-478.
- Suzuki, D. A., Yamada, T., Hoedema, R., & Yee, R. D. (1999). Smooth-pursuit eye-movement deficits with chemical lesions in macaque nucleus reticularis tegmenti pontis. *J Neurophysiol*, *82*(3), 1178-1186.
- Takagi, M., Zee, D. S., & Tamargo, R. J. (1998). Effects of Lesions of the Oculomotor Vermis on Eye Movements in Primate: Saccades. *J Neurophysiol*, *80*(4), 1911-1931.

- Tanaka, K., Sugita, Y., Moriya, M., & Saito, H. (1993). Analysis of object motion in the ventral part of the medial superior temporal area of the macaque visual cortex. *J Neurophysiol*, 69(1), 128-142.
- Tanaka, M. (2005). Involvement of the central thalamus in the control of smooth pursuit eye movements. *J Neurosci*, 25(25), 5866-5876.
- Tanaka, M., & Lisberger, S. G. (2001). Regulation of the gain of visually guided smooth-pursuit eye movements by frontal cortex. *Nature*, 409(6817), 191-194.
- Tanaka, M., & Lisberger, S. G. (2002a). Enhancement of multiple components of pursuit eye movement by microstimulation in the arcuate frontal pursuit area in monkeys. *J Neurophysiol*, 87(2), 802-818.
- Tanaka, M., & Lisberger, S. G. (2002b). Role of arcuate frontal cortex of monkeys in smooth pursuit eye movements. I. Basic response properties to retinal image motion and position. *J Neurophysiol*, 87(6), 2684-2699.
- Tanaka, M., & Lisberger, S. G. (2002c). Role of arcuate frontal cortex of monkeys in smooth pursuit eye movements. II. Relation to vector averaging pursuit. *J Neurophysiol*, 87(6), 2700-2714.
- Thier, P., & Ilg, U. J. (2005). The neural basis of smooth-pursuit eye movements. *Curr Opin Neurobiol*, 15(6), 645-652.
- Thomas, N. W., & Pare, M. (2007). Temporal processing of saccade targets in parietal cortex area LIP during visual search. *J Neurophysiol*, 97(1), 942-947.
- Thompson, K. G., Bichot, N. P., & Schall, J. D. (1997). Dissociation of visual discrimination from saccade programming in macaque frontal eye field. *J Neurophysiol*, 77(2), 1046-1050.
- Thompson, K. G., Hanes, D. P., Bichot, N. P., & Schall, J. D. (1996). Perceptual and motor processing stages identified in the activity of macaque frontal eye field neurons during visual search. *J Neurophysiol*, 76(6), 4040-4055.
- Tian, & Lynch, J. C. (1997). Subcortical input to the smooth and saccadic eye movement subregions of the frontal eye field in Cebus monkey. *J Neurosci*, 17(23), 9233-9247.
- Tian, J. R., & Lynch, J. C. (1996a). Corticocortical input to the smooth and saccadic eye movement subregions of the frontal eye field in Cebus monkeys. *J Neurophysiol*, 76(4), 2754-2771.
- Tian, J. R., & Lynch, J. C. (1996b). Functionally defined smooth and saccadic eye movement subregions in the frontal eye field of Cebus monkeys. *J Neurophysiol*, 76(4), 2740-2753.
- Treisman, A., & Gormican, S. (1988). Feature analysis in early vision: evidence from search asymmetries. *Psychol Rev*, 95(1), 15-48.
- Treue, S., & Maunsell, J. H. (1999). Effects of attention on the processing of motion in macaque middle temporal and medial superior temporal visual cortical areas. *J Neurosci*, 19(17), 7591-7602.
- Treue, S., Hol, K., and Rauber, H. J. (2000). Seeing multiple directions of motion - Physiology and psychophysics. *Nat Neurosci*, 3(3), 270-276
- Wall, J.T., Symonds, L.L., Kaas, J.H. (1982). Cortical and subcortical projections of the middle temporal area (MT) and adjacent cortex in galagos. *J Comp Neuro*, 211(2), 193-214.
- Wardak, C., Olivier, E., & Duhamel, J. R. (2002). Saccadic target selection deficits after lateral intraparietal area inactivation in monkeys. *J Neurosci*, 22(22), 9877-9884.
- Wurtz, R. H., & Hikosaka, O. (1986). Role of the basal ganglia in the initiation of saccadic eye movements. *Prog Brain Res*, 64, 175-190.

- Yamada, T., Suzuki, D. A., & Yee, R. D. (1996). Smooth pursuitlike eye movements evoked by microstimulation in macaque nucleus reticularis tegmenti pontis. *J Neurophysiol*, 76(5), 3313-3324.
- Zee, D. S., Yamazaki, A., Butler, P. H., & Gucer, G. (1981). Effects of ablation of flocculus and paraflocculus of eye movements in primate. *J Neurophysiol*, 46(4), 878-899.